AD NUMBER
AD325537
CLASSIFICATION CHANGES

TO:	unclassified
FROM:	restricted

LIMITATION CHANGES
TO:
Approved for public release; distribution is unlimited.
FROM:
Controlling Organization: British Embassy, 3100 Massachusetts Avenue, NW, Washington, DC 20008.
AUTHORITY
DSTL, DEFE 15/960, 11 Dec 2008; DSTL, DEFE 15/960, 11 Dec 2008

U.S. CONFIDENTIAL — Modified Handling Authorized
U.K. RESTRICTED
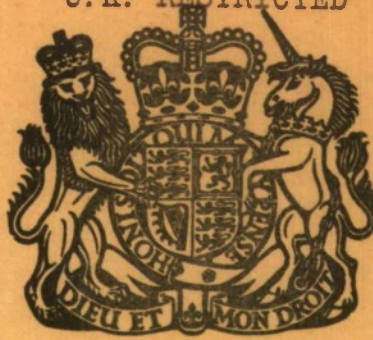
AD325537

Decl OADR

f EXCLUDED FROM AUTOMATIC
REGRADING; DOD DIR 5200.10
DOES NOT APPLY REVIEWED ON:

_____
Date   Signature

ARMAMENT RESEARCH AND DEVELOPMENT

ESTABLISHMENT

89995

BASIC RESEARCH AND WEAPON SYSTEMS ANALYSIS DIVISION

20080730 207

A.R.D.E. MEMORANDUM (B) 49/61

Some experiments on hypervelocity impact

U.S. CONFIDENTIAL — Modified Handling Authorized
U.K. RESTRICTED
W. A. Clayden

Fort Halstead,
Kent

September
1961

C88995 (all) 110

(ARMAMENT RESEARCH AND DEVELOPMENT ESTABLISHMENT. G. B.)

A.R.D.E. MEMORANDUM (B) 49/61

(Some experiments on hypervelocity impact)

(W.A. Clayden) (B3)

(Sept 1961)

Summary

     Crater dimensions have been obtained in various metal targets when attacked by $\frac{1}{4}$ in. diameter spheres with velocities up to 10,000 ft/sec. The depth of penetration in 'semi-infinite' targets attacked at normal incidence has been correlated with an empirical formula which is in agreement with existing work. When the semi-infinite targets were attacked at incidence the depth of penetration was found to be proportional to the sine of the angle of incidence. When thin targets were attacked at incidence the crater dimensions were similar to those obtained for 'semi-infinite' targets inclined at the same angle provided the thin targets were not penetrated. An empirical relationship is given for a minimum thickness of target for non-penetration as a function of the impact velocity, the properties of the target and projectile and the angle of incidence.

Approved for issue:

     J.W. Maccoll, Principal Superintendent 'B' Division

INITIAL DISTRIBUTION

Internal

No. 1	Director
2	Deputy Director
3	PS/B
4	PS/L
5	PS/MX
6	PS/P
7	Dr. W.M. Evans
8	S/B3
9	S/B1
10	S/B2
11	S/X1
12-14	B3 (Att. Dr. R.N. Cox, Mr. W.A. Clayden, Mr. C. Vincent)
15-16	B2 (Att. Mr. A.D. Cox, Mr. S.J. Tupper)
17	M2 (Att. Dr. S.C. Hunter)
18-19	B Division Library

External UK

20	Chief Scientist M of A
21	Chief Scientist WO
22	Deputy Chief Scientist (A)
23	DG of A/Admin.
24	D of A (R and D)
25-26	NPL (Att. Dr. M.P. Musgrave, Mr. H.L. Cox)
27-51	Secretary, Mathematics and Physics Committee, SAC
52	Secretary, OB

Universities

53	Cambridge - (Att. Dr. F.P. Bowden, F.R.S.)
54	Glasgow - Royal College of Science and Technology (Att. Prof. D.C. Pack)
55	Nottingham - (Att. Dr. A.J.M. Spencer)
56	Sheffield - (Att. Dr. P. Chadwick)
57-58	TIL - for retention

Overseas (through TIL)

59	DRS (Att. Director of Munitions)
60	Defence Research and Supply Liaison Office, U.K. High Commission, Ontario (Att. Mr. C.J. Francis)
61-65	Canada - Dept. Nat. Def.
66	- Nat. Res. Council
67-70	- Def. Res. Liaison
71-72	- CARDE (Att. Mr. C.J. Maiden, Mr. H.P. Tardif)
73	- CALE

RESTRICTED

74-78	Australia – Sen. Rep.
79	– RAAF Overseas HQ., London
80-97	USA – Joint Reading Panel
98	– Assist. Sec. of Def. for Res. and Dev.
99-100	– ONR (London)
101-102	– BRL Aberdeen Proving Ground, Maryland (Att. Technical Director, Dr. Lampson)
103-105	– NOL Silver Spring, Maryland (Att. Technical Director, Dr. Hartmann, Dr. A.D. Solem, Explosives Dept.)
106-108	– NOTS Inyokern, California (Att. Dr. W.A. Allen, Dr. J. Pearson, Dr. B.E. Drimmer)
109	– NRL Washington 25, D.C. (Att. Dr. W.W. Atkins)
110	– WAL Watertown Arsenal, Mass. (Att. Dr. K.H. Abbott)
111	– NASA Ames Research Center, California (Att. Dr. A.C. Charters)
112	– Picatinny Arsenal, N.J. (Att. Dr. E.N. Clark)
113	– Colorado School of Mines (Att. Dr. J.S. Rinehart)
114-115	– The RAND Corporation, Santa Monica, California (Att. Dr. R.L. Bjork, Dr. B.R. Parkin)
116-117	– Poulter Labs., Menlo Park, California (Att. Dr. T.C. Poulter, Dr. G.E. Duval)
118-119	– ARO Inc., PO Box 162, Tullahoma, Tennessee (Att. Library, Gas Dynamics Facility)
120	– Arthur D. Little, Inc. Acron Park, Mass. (Att. Dr. D.B. Lull)
121	– Space Technology Labs. Inc., Los Angeles, California
122	– Armour Research Foundation, Chicago (Att. Dr. S. Okubo)
123	– University of Utah, Salt Lake City (Att. Dr. R.W. Crow, (High Velocity Lab.))
124	– Massachusetts Institute Technology, Lexington, Mass. Lincoln Lab. (Att. Dr. W.G. Clay)
125-126	France – Institut de Recherches de Saint Louis (Att. Prof. H. Schardin)

Stock

127-136

List of Symbols

b	target thickness
b*	minimum target thickness for non penetration
c_p	speed of sound in the projectile given by $\sqrt{E_p/\rho_p}$
c_t	speed of sound in the target given by $\sqrt{E_t/\rho_t}$
D	diameter of the crater in the plane of the undisturbed surface of the target
d	diameter of the projectile
d_p	shock speed in the projectile
d_t	shock speed in the target
d_1	thickness of a one dimensional projectile
E_p	Youngs modulus for the projectile
E_t	Youngs modulus for the target
L	length of crater formed at oblique impact
L'	length of damaged region formed at oblique impact
P	depth of penetration
δP	thickness of projectile at the bottom of a crater after impact
y	distance of a point in a target from the apparent centre of expansion
δy	deformation in a target
t	time
U	impact velocity
u	interface velocity
V	crater volume
δV	volume of that part of the crater contributing to a spherical deformation
v	projectile volume
v_1	volume of a one calibre cylindrical projectile
x	distance of a point in the target from the apparent centre of expansion, measured in a direction parallel to the undisturbed surface
δx	deformation in the x direction
y	distance of a point in the target from the apparent centre of expansion, measured in a direction perpendicular to the undisturbed surface

δy deformation in the y direction

ϵ strain

ϵ_x strain in the x direction

ϵ_y strain in the y direction

θ angle between the line of flight of the projectile and the surface of the target

ρ_p density of the projectile

ρ_t density of the target

1. Introduction

Impact phenomena at high speeds have recently become important because of the desire to obtain some understanding of the damage which will be sustained by the skin of a missile or space vehicle when struck by fragments of meteorites. More basic information on the behaviour of materials when subjected to very high loads may also be obtained.

The general problem of the damage sustained by a plate when struck by a fragment at high velocity contains a vast number of parameters and there does not yet appear to be an adequate theory or even a complete understanding of the physical processes. The comparatively simple case of a crater formed in a semi-infinite target when struck by a sphere at normal incidence has been studied experimentally by a number of workers and several empirical laws relating the penetration to the impact Mach number (ratio of the velocity of the projectile relative to the target/speed of sound in the target given by $\sqrt{E_t/\rho_t}$) have been proposed. This work has been extended at ARDE and this memorandum contains an account of some experiments which were undertaken during the latter part of 1959 to show the general trend of damage which might result as the shape of the fragment, the angle of impact and the thickness of the target were varied.

2. Experimental Technique

2.1 Launcher

The projectiles were fired with the ARDE two stage light gas gun the performance of which is described in detail in ref.1. Briefly this gun has a $\frac{1}{4}$ in. launcher barrel and a 1 in. compressor barrel and compressed helium is used to drive a light polythene piston along the compressor barrel compressing helium to very high pressures and temperatures. This high pressure helium is then used to launch $\frac{1}{4}$ in. diameter models at speeds in excess of 10,000 ft/sec. The velocity of the projectile was measured in this series of tests by firing the projectiles through a number of stations each of which consisted of two sheets of aluminium foil which acted as a make circuit as the projectile passed through. The output of these screens was displayed on a spiral base oscilloscope and the impact velocity was then obtained from the velocity between the screens by applying a correction for air drag. Several projectiles were recovered after firing through the screens into water and a comparison of the weights of the projectiles before and after firing showed that the loss of mass due to the combined effects of passing through several foils and erosion in the launcher barrel was less than 1 per cent.

2.2 Targets

The 'semi-infinite' targets were mainly 4 in. in diameter and 2 in. thick and were mounted so that the incidence could be easily adjusted. The thin targets were 4 in. square and were mounted in a similar manner. The crater volumes were measured by filling the crater with water from a burette to a level corresponding to the undisturbed surface of the target. The water had a small amount of detergent added to reduce the surface tension. The depth of the crater from the undisturbed surface was measured with an engineers depth micrometer. The diameter of the crater in the plane of the undisturbed surface was measured with a pair of inside vernier callipers; several readings were taken at different diameters and the readings were averaged. In the case of the craters formed at small angles of incidence the edges of the crater were not well defined and the major and minor axes were measured with a steel rule. In some circumstances (e.g. when aluminium projectiles were fired into lead targets at low speeds) the deformed projectile fell out of the crater and measurement of the crater in the target presented no particular difficulties. When the deformed projectile attached itself

1

firmly to the crater however and particularly when the volume of the projectile was comparable with that of the crater (e.g. the case of the aluminium cylinders into aluminium targets) the above simple procedure had to be modified and typical craters were sectioned and etched. This process clearly showed the dividing line between the projectile and target and measurements of the depth of penetration and the diameter were then corrected to allow for the thickness of the deformed projectile spread over the crater wall. However at impact speeds of 10,000 ft/sec this correction was smaller than the experimental error. The volume of the crater in the target alone was obtained by measuring the volume of the crater when containing the deformed projectile and adding on the volume of the projectile.

3. Results

3.1 Impact of spheres into semi-infinite targets at normal incidence

Figs. 1 and 2 show the results of firing $\frac{1}{4}$ in. aluminium spheres into lead and aluminium targets at impact speeds between 2,000 and 10,000 ft/sec. These results illustrate some of the general features of high speed impact into ductile metal targets:

(1) As the impact speed increases so the shape of the crater tends to become hemispherical.

(2) For given projectile and target materials the volume of the crater is proportional to the kinetic energy of the projectile.

(It is interesting to note that at speeds of the order of 10,000 ft/sec the kinetic energy per pound of projectile is of the same order as the chemical energy per pound of explosive.)

No adequate underlying theory exists for impact in this speed range, but several workers (e.g refs. 2 and 3) have attempted to relate the penetration of spheres to the velocity of impact and the target properties with a simple empirical formula of the form

$$\frac{P}{d} = k \left(\frac{U}{c_t}\right)^n \left(\frac{\rho_p}{\rho_t}\right)^m , \qquad (1)$$

where P is the penetration, d is the diameter of the projectile, k, n and m, are constants, U is the velocity of impact, c_t is the speed of sound in the target given by $\sqrt{E_t/\rho_t}$ and ρ_p and ρ_t are the densities of the projectile and target respectively. Some of these formulae are compared in fig. 3 and for engineering purposes these formulae are probably adequate for the limited range of velocities and materials for which they were derived. The reason for the apparent dependence of the depth of penetration on the density ratio and the "impact Mach number" (U/c_t) is not yet properly understood but some plausible explanation may be sought by considering a one dimensional impact problem of a slab of density ρ_p and thickness of d_1 striking a stationary semi-infinite target of density ρ_t. After impact the interface will move into the stationary target with a velocity U which may be obtained by equating the pressures on either side of the interface thus

$$\rho_t u d_t = \rho_p (U-u) d_p$$

where d_t and d_p are the shock speeds in the target and projectile respectively.

Hence

$$u = \frac{\rho_p c_p}{\rho_t c_t + \rho_p c_p} \cdot U .$$

[If the projectile and target are of the same material then $u = \dfrac{U}{2}$ a result which follows from considerations of symmetry.] Now the depth of penetration will be given by $P = u\,t$ where t is the time taken for the shock from the interface to travel to the free surface of the slab and reflect back again as a rarefaction. At impact speed of the order of 10,000 ft/sec. t is approximately equal to $2d_1/c_p$ and hence the non dimensional penetration may be written as

$$\frac{P}{d} = \frac{2}{c_p}\,\frac{\rho_p c_p U}{(p_t c_t + \rho_p c_p)}$$

which may be rearranged to give

$$\frac{P}{d} = \left[\frac{U}{c_t}\right]\left[\frac{\rho_p}{\rho_t}\right]\left\{\frac{2}{1 + \dfrac{\rho_p c_p}{\rho_t c_t}}\right\} \qquad (2)$$

For most combinations of common metals the quantity in curly brackets will not differ from unity by more than about 3 per cent. For the three-dimensional case the penetration will be considerably greater because the target material is able to flow away from the projectile.

The penetration results shown in figs. 1 and 2 and the results of a systematic series of firings in which aluminium spherical projectiles were fired at a speed of 10,000 ft/sec into various targets are plotted against $\left[\dfrac{\rho_p}{\rho_t}\right]\left[\dfrac{U}{c_t}\right]$ in fig.3. and compared with previous results. These results which were obtained for 8 widely differing combinations of projectile and target material do not deviate by more than 30 per cent from a mean line given by

$$\frac{P}{d} = 2{\cdot}0\,\left(\frac{\rho_p}{\rho_t}\right)^{\frac{2}{3}}\left(\frac{U}{c_t}\right)^{\frac{2}{3}} \qquad (3)$$

and apart from a constant of 2 instead of 2.28 this is similar to the relationship obtained by Charters and Locke; in fact our results for aluminium and lead targets are fitted slightly better by the Charters and Locke formulae. A deviation of as much as 30 per cent however is considerably more than would be expected by experimental error alone and it now seems likely from the growing volume of experimental data that whilst the correlation given by equation (3) may be sufficient for engineering purposes for a limited range of velocities and materials it does not contain all the relevant parameters to explain all the phenomena. The correlation of the data in fig.3 was not improved when plotted against the parameter

$$\left[\frac{U}{c_t}\right]\left[\frac{\rho_p}{\rho_t}\right]\left\{\frac{2}{1 + \dfrac{\rho_p c_p}{\rho_t c_t}}\right\}$$

suggested by the R.H.S. of equation (2) for one dimensional penetration. The $\frac{2}{3}$ power in equation (3) has a physical significance because it seems to be well established that at speeds of the order of 10,000 ft/sec. the crater becomes hemispherical and the volume is proportional to the energy

thus $\qquad\qquad\qquad V \propto PD^2 \propto P^3$ and $V \propto U^2$

hence $\qquad\qquad\qquad P \propto U^{2/3}$.

When the depth of penetration is compared on the basis of equation (3) there does not appear to be any marked difference between the ductile materials such as aluminium and copper and the brittle materials such as cast iron and titanium nevertheless the craters are completely different. Fig.4 illustrates typical craters formed in various materials ranging from very ductile aluminium to brittle perspex. It may be seen that in the case of the aluminium target the target has undergone considerable plastic deformation but has lost very little material, whereas in the case of the cast iron target there is little plastic flow and most of the material from the crater has been lost. This is because in a brittle material the dynamic hoop stress produced by the impact causes extensive cracking and small fragments fall away from the target. It appears therefore that when considering the damage to brittle materials the size of the crater is probably unimportant and the extent of the cracking should be taken into account, this is particularly well illustrated in fig.4e. where the radius of damage in the perspex target is about six times that of the crater. The elektron target shows that it is possible to have considerable plastic deformation and cracking together. The reason for the conical crater in titanium (this effect is repeatable) is not obvious but an examination of an etched specimen shows that the region of deformation and cracking is roughly hemispherical.

Fig.5 shows the magnitude and direction of the plastic deformation of the aluminium target and when these vectors are projected they appear to intersect at approximately the same point. Taking this point as an origin the deformations, δx and δy, and strains, ϵ_x and ϵ_y, in the horizontal and vertical planes respectively have been plotted in fig.6 as a function of x and y. These curves show that below a horizontal plane through the origin the target deformation is spherically symmetrical. Qualitatively it appears that the top part of the material from the crater has gone into the 'splash' and in deforming the free surface whilst the bottom part has deformed the whole target in a similar manner to a spherical expansion. By considering conservation of mass across a spherical surface centred at the origin the deformation of the target δr may be expressed in terms of the radius r and the volume of the lower part of the crater δr, thus

$$\delta V = \frac{2}{3} \pi \left\{ (r + \delta r)^3 - r^3 \right\}$$

which may be written as

$$(\delta r)^3 + 3r (\delta r)^2 + 3r^2 (\delta r) - \frac{3\delta V}{2\pi} = 0. \qquad (4)$$

This curve has been fitted to the experimental points in fig.6a and it may be seen that the fit is good. The ratio of the volume of the lower part of the crater δV to the total volume of the crater V is about one third for this target. At large distances from the crater the deformation is given approximately by

$$\delta r = \frac{\delta V}{2\pi r^2} \qquad (5)$$

The strain may be obtained from (4) by writing

$$\epsilon = \frac{d(\delta r)}{dr}$$

and this curve has been drawn through the experimental points in fig.6b and again the fit is good. At large distances from the crater the strain is given approximately by

$$\epsilon = \frac{-\delta V}{\pi r^3} \qquad (6)$$

4

Applying (6) to the aluminium target and taking the limit of plastic flow to be given by $\epsilon = 0.001$, plastic flow will have extended to over 2 in. from the centre of the crater. The analysis given above does not appear to be applicable to the other targets in view of the lack of symmetry and the loss of material from the crater but the displacements and strain for the Elektron and cast iron targets are shown in fig.7. The relationship given by equation (6) may be used to obtain an estimate of the size of a target which is required before it may be considered semi-infinite and for this purpose δV may be replaced by an estimated V.

3.2 Impact of spheres into semi-infinite targets at varying angles of incidence

Fig.8 illustrates the results of firing $\frac{1}{4}$ in. spherical aluminium projectiles at impact speeds of 10,000 ft/sec into 'semi-infinite' copper targets with the surface inclined at angles between 10° and 90° to the line of flight of the projectile. The results show that the penetration is approximately proportional to the sine of the angle of incidence and for engineering purposes the results may be fitted quite well by

$$\frac{P}{d} = (\frac{P}{d} \text{ at } 90^\circ \text{ incidence}) \sin \theta \text{ * .}$$

The area of the crater remains roughly constant and the volume follows a similar trend to the penetration and may be fitted by $\frac{V}{v} = (\frac{V}{v} \text{ at } 90^\circ$ incidence) $\sin^2 \theta$. At small angles of incidence the crater consists of one main cavity and a series of subsidiary cavities as though the projectile had formed several small drops soon after impact each of which had gone on to form a cavity. At small angles of incidence also the length of these chains of craters tends to become equal to the length of the diameter of the projectile projected on to the target surface. This might be expected since the projectile tends to simply smear itself along the surface leaving only a very small impression. At small angles of incidence the crater is by no means well defined and the crater parameters for angles of less than 30° are to be used with caution.

At normal angles of impact there is evidence to show that the crater dimensions can be correlated on a basis of impact Mach number as discussed in section 3.1 and hence to simulate very high speed impact the above series was repeated using lead targets and the results are shown in fig.9. Somewhat similar results are obtained but in this case the crater is not dependent upon the angle of impact in the range 60° to 90° and at small angles of incidence a well defined crater is formed with a lip on one side (in fig. 9 L' is the length of the crater whilst L is the length of the damaged region). The differences between the lead and copper targets are illustrated in fig.10.

A third series of tests was performed in which the impact angle was held constant at 20° and the projectile velocity varied from 3,000 to 10,000 ft/sec. and the results are shown in fig.11. The most striking feature of these tests is shown in fig.12 where it may be seen that as the impact speed increases the crater changes shape from a shallow smear to become almost axisymmetric with only a small 'splash' on one side to indicate that the projectile has not entered at normal incidence, further at all speeds the deepest part of the cavity is towards the launcher. Under

---

*A similar relationship is given in ref.8 for steel fragments into lead targets at impact speeds of 15,000 ft/sec.

these conditions it is interesting to note that the penetration is proportional to the impact velocity and the crater volume is proportional to the energy as in the case of normal incidence impact at low speeds. There seems little doubt from the evidence in fig.12 that if the speed were increased still further the crater would become completely axisymmetric,* and it is interesting to speculate whether under these conditions the crater size and shape would tend to equal that produced by normal impact; or in other words would the crater formed at very high speed impact depend only on the energy and be independent of incidence.

3.3 Impact of cylinders into 'semi-infinite' targets at normal incidence

Fig.13 gives the crater dimensions as a function of length for tests in which $\frac{1}{4}$ in. diameter aluminium cylinders were fired into semi-infinite targets at normal incidence at impact speeds of 4,000 and 7,000 ft/sec. The deformed projectile occupied a considerable part of the crater in the target and the dimensions of the crater in the target alone and the crater plus deformed projectile are shown for comparison. Each test point represents the average of several separate firings.

For small values of l/d it might be expected that the penetration of the cylinders would tend towards a value given by equation (2) for one-dimensional impact and that for large values of l/d the penetration would tend towards that of a hydrodynamic jet which has been studied by Hill, Mott and Pack (ref.4). These theories are shown in fig.13 together with an empirical relation devised by Kinard and Lambert (ref.5) for the penetration of steel cylinders of 0.5 and 1 calibre into copper targets. It may be seen from Fig.13 that the measured penetration does not tend towards the expected limits and further the penetration is not proportional to the length of the projectile which is also predicted by these relationships. Sections through the targets (Fig.14) show how the crater gradually changes from one with a comparatively shallow flat bottom which would be expected if the target was struck by a thin disc when the flow would be approximately one-dimensional to a deep rounded crater which would occur if the target was struck by a long jet. The impact of one calibre aluminium cylinders has been studied theoretically at much higher velocities by Bjork, ref.6 and these results are compared with the ARDE results at lower velocities and an experimental result attributed to Atkins in fig.15. In the speed range of 4,000 to 18,000 ft/sec. the experiments show that $P \propto U^{2/3}$ but Bjork's theory shows that if this law was used to estimate damage at significantly higher speeds the depth of penetration would be over-estimated by a factor of 2 or 3 ** .

3.4 Impact of spheres into thin targets at normal incidence

Fig.16 shows the crater radius as a function of plate thickness for copper and lead plates when attacked by aluminium projectiles at 10,000 and 9,000 ft/sec respectively. This shows that the crater radius increases from the projectile radius for very thin targets to slightly

---

* It is suggested in ref.9 that hemispherical craters will always be formed provided the normal component of impact velocity is greater than the dilational wave speed in the target.

** Recent work with micro particles impacting at speeds of 30,000 ft/sec tend to confirm the $^2/_3$ power law however (ref.10)

more than the radius of the crater formed in a semi-infinite target when
the plate is just not penetrated. Another important feature of a plate
which is just not penetrated is that the depth of penetration is considerably
greater than in the semi-infinite target. This fact should be borne in
mind if the vulnerability of a thin skin to attack by fragments is to be
assessed from penetration data derived from thick targets.

Several very thin lead and copper targets were weighed before and
after impact and it was found that the loss of material was roughly equal
to a disc of similar size to the crater and there was little plastic flow
in the remaining part of the target. This is illustrated in fig.17a which
shows that there is no measurable distortion in the grid which was scribed
on a thin lead target before impact. As the thickness of the target was
increased, however, a considerable amount of plastic flow occurred and
the back of the target was damaged by a phenomena known as scabbing shown
in figs. 17b and c. This phenomena is caused by a compression wave,
initiated by the impact, reflecting from the free surface as a tension
wave and tearing the material apart. Since lead is relatively weak in
tension this effect was much more pronounced in the lead targets than in
the copper targets.

3.5 Impact of spheres into thin targets at incidence

Fig.18 shows the results of firing $\frac{1}{4}$ in. spherical aluminium
projectiles at impact speeds of 10,000 ft/sec into thin copper targets
with the surface inclined at various angles between 10° and 90° to the line
of flight of the projectile. The results show that the depth of penetration
when defined as shown in fig.18 is slightly less than in a semi-infinite
target presumably because some of the energy of the projectile has gone
into bending the plate. The remarks in section 3.2 concerning the crater
shape are still applicable and as shown in fig.18 the crater shape is
very similar to the semi-infinite case. These tests were repeated for
a series of thin lead plates and the results are shown in fig.19.

From a study of steel spheres attacking copper plates at velocities
between 4,000 and 11,500 ft/sec. Kinard et al, ref.7 concluded that the
minimum thickness that will not be penetrated, b*, was given by

$$\frac{b^*}{d} = 3.47 \left(\frac{U}{c_t}\right) \left(\frac{\rho_r}{\rho_t}\right) . \qquad (7)$$

Since the depth of penetration is approximately proportional to the sine
of the angle of incidence it seems reasonable to extend equation (7) to
give a criterion for penetration for inclined plates which may be written
as

$$\frac{b^*}{d} = 3.47 \left(\frac{U}{c_t}\right) \left(\frac{\rho_p}{\rho_t}\right) \sin \theta . \qquad (8)$$

This empirical relation, shown in figs.18 and 19, separates the plates
which were penetrated from those that were not except for one.

' The results in section 3.1 show that the depth of penetration of
spheres into semi-infinite targets at normal incidence is proportional to
the velocity raised to the power of two thirds, so far consistency with
this relationship a better criterion for penetration of thin inclined
plates might be expected to be of the form

$$\frac{b^*}{d} = k\left(\frac{U}{c_t}\right)^{2/3} \left(\frac{\rho_p}{\rho_t}\right)^{2/3} \sin \theta . \qquad (9)$$

The best fit to the results shown in figs.18 and 19 is obtained with
k = 2.75 and this relationship is also shown in these figs. It must be

admitted, however, that the two third powers in (9) cannot be justified from the results into inclined plates as these were all performed at one velocity.

4. Conclusions

Crater dimensions have been obtained in various metal targets when attacked by $\frac{1}{4}$ in. diameter spheres with velocities up to 10,000 ft/sec and the penetration correlated approximately with the relationship

$$\frac{P}{d} = 2.0 \left(\frac{\rho_p}{\rho_t}\right)^{2/3} \left(\frac{U}{c_t}\right)^{2/3}$$

which is in reasonable agreement with much of the existing work. The deviation of the experimental points from this empirical relationship is more than can be attributed to experimental error and whilst it may be adequate for the practical problem of damage assessment within a limited range of velocities and materials it is not adequate to explain the whole phenomena of impact. The penetration of brittle targets may be estimated with the above formula but this is of little use in assessing damage since a region of severe cracking may surround the crater. The deformation surrounding the crater in a ductile aluminium target was spherically symmetrical about a point below the target surface apart for a small region extending to half the depth of the crater just below the surface. This fact enables the extent of plastic flow in a ductile target to be readily determined and hence the size of target required for a particular experiment may be estimated.

When $\frac{1}{4}$ in. aluminium spheres were fired into inclined lead and copper targets at 10,000 ft/sec the depth of penetration was roughly proportional to the sine of the angle of incidence and the volume was proportional to the square of the sine of the angle of incidence. When lead targets were attacked at a constant angle of incidence of 20° with $\frac{1}{4}$ in. aluminium spheres the crater tended to become axially symmetric as the impact speed increased to 12,000 ft/sec indicating that if a crater was caused by a meteorite moving at speeds of several times this value it would in all probability be completely symmetrical for all but very small angles of incidence. Even though the angle of incidence was 20° the penetration was proportional to the impact velocity and the crater volume proportional to the kinetic energy.

The crater dimensions in aluminium targets were obtained when attacked by various lengths of $\frac{1}{4}$ in. diameter aluminium cylinders at speeds of 4,000 and 7,000 ft/sec. The penetration was compared with theoretical predictions for the extreme cases of a very short cylinder (one dimensional impact) and a very long cylinder (a jet). These theories and a previous empirical result predict that the penetration will be proportional to the length of the projectile whereas the experimental points do not show this trend and also do not tend towards the expected limits.

Thin lead and copper targets were attacked by $\frac{1}{4}$ in. aluminium spheres at 10,000 ft/sec at normal incidence and it was found that the crater diameter increased with the target thickness and in some circumstances became greater than in a semi-infinite target. Projectiles completely penetrated targets whose thickness was significantly greater than the depth of penetration of a similar projectile in a semi-infinite target; this was partly due to the phenomena of scabbing whereby the compression wave from the impact is reflected from the back of the target as a tension wave and the back of the target then fails under tension. This effect was much more pronounced with the lead targets as lead is weak in tension. Crater (complete perforations) in thin targets (thickness less than half the depth of penetration in a semi-infinite target) were caused by loss of material rather than any

significant plastic flow. When these targets were attacked at incidence the crater dimensions were similar to those obtained for semi-infinite targets provided the target was not penetrated. A minimum thickness of target for non penetration, b*, is given by the following empirical relationship

$$\frac{b^*}{d} = 2.75 \left(\frac{U}{c_t}\right)^{2/3} \left(\frac{\rho_p}{\rho_t}\right)^{2/3} \sin \theta$$

but due to the increased complexity of the problem of damage to an inclined thin target the remarks at the beginning of this section concerning the empirical formula for penetration of a semi-infinite target are even more valid.

References

1. W.A. Clayden
    D.F.T. Winter and
    F. Swan
    "The ARDE hypervelocity launcher".
    9th Tripartite AXP Research Conference,
    Canada, April 1959.

2. M.E. van Valkenburg,
    G. Clay and
    J.H. Huth
    "Impact phenomena at high speeds".
    Jour. App. Phys., vol. 27, No.10,
    October 1956.

3. J.L. Summers and
    A.C. Charters
    "High speed impact of metal projectiles in
    targets of various materials".
    Proc. Third Symposium on Hypervelocity
    Impact, October 1958.

4. D.C. Pack and
    W.M. Evans
    "Penetration by high-velocity ('Munroe')
    jets".
    Proc. Phys. Soc., B, Vol.64, No.4.

5. W.H. Kinard and
    C.H. Lambert, Jr.
    "An investigation of the effect of target
    temperature on projectile penetration and
    cratering".
    NACA RM L58E 14, July 1958.

6. R.L. Bjork
    "Effects of a meteoroid impact on steel and
    aluminium in space".
    10th International Astronautical Congress,
    August 1959.

7. W.H. Kinard
    C.H. Lambert, Jr.
    D.R. Schrejer and
    F.W. Casey, Jr.
    "Effect of target thickness on cratering
    and penetration of projectiles impacting
    at velocities to 13,000 feet per second".
    NASA memo. 10-18-58L, December 1958.

8. J.H. Kineke, Jr.
    "An experimental study of crater formation
    in metallic targets".
    Fourth Symposium on Hypervelocity Impact,
    April, 1960.

9. J.W. Gehring, Jr.
    "Observations of the phenomena of hypervelocity
    impact".
    Fourth Symposium on Hypervelocity Impact,
    April 1960.

10. J.W. Gehring, Jr. and
    L.G. Richards
    "Further studies of micro-particle cratering
    in a variety of target materials".
    Fourth Symposium on Hypervelocity Impact,
    April, 1960.
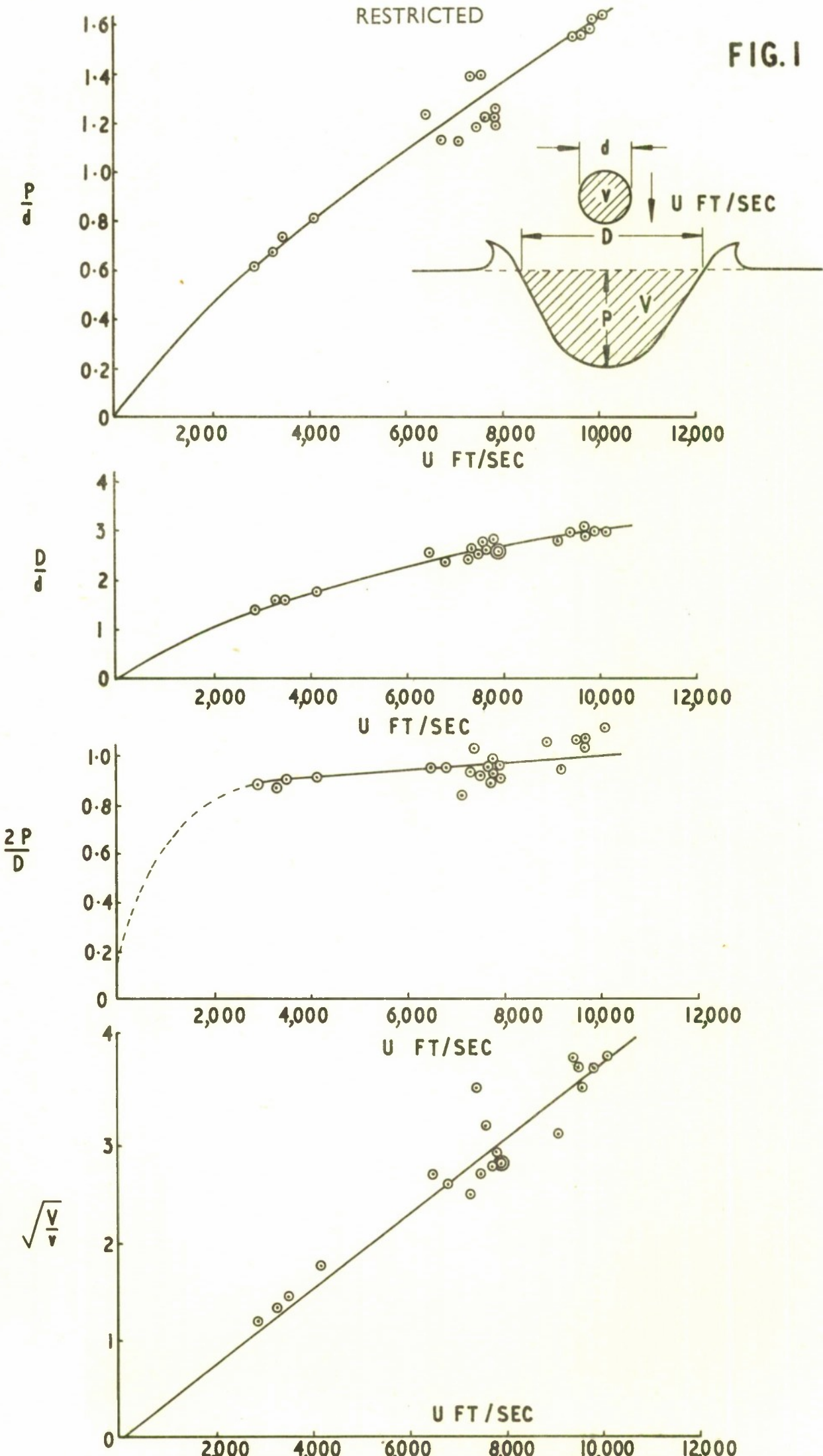
FIG. I CRATER DIMENSIONS AS A FUNCTION OF IMPACT VELOCITY, ¼" ALUMINIUM SPHERES INTO ALUMINIUM TARGETS AT NORMAL INCIDENCE
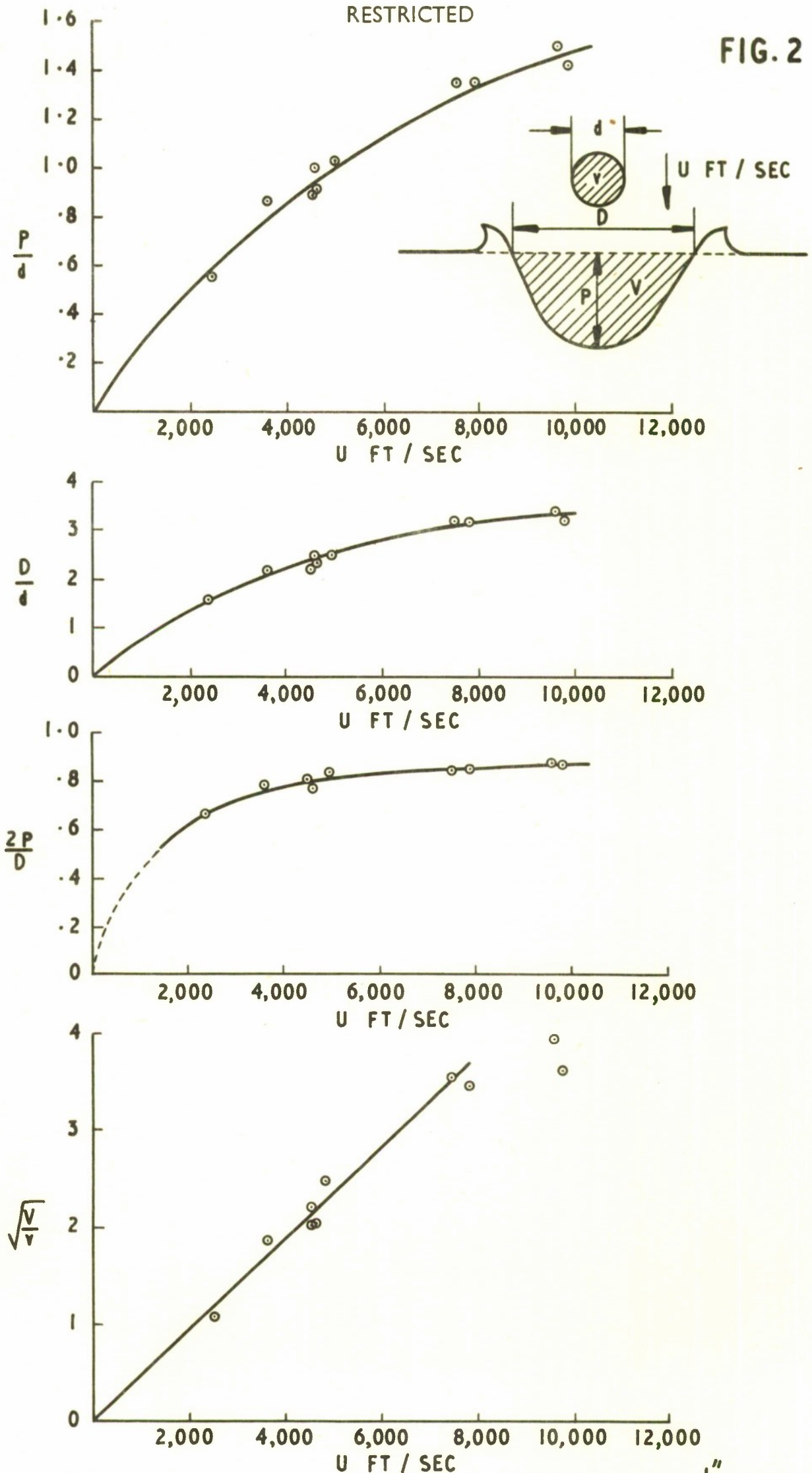
FIG. 2

FIG. 2 CRATER DIMENSIONS AS A FUNCTION OF IMPACT VELOCITY—$\frac{1}{4}''$ ALUMINIUM SPHERES INTO LEAD TARGETS AT NORMAL INCIDENCE

FIG. 3

$$\frac{P}{d} = 2.28 \left(\frac{\rho_p}{\rho_t}\right)^{0.69} \left(\frac{U}{C_t}\right)^{0.69}$$ ----------- CHARTERS AND LOCKE

$$\frac{P}{d} = 2.18 \left(\frac{\rho_p}{\rho_t}\right)\left(\frac{U}{C_t}\right)$$ ——x——x——x—— KINARD AND LAMBERT

$$\frac{P}{d} = 2.5 \left(\frac{U}{C_t}\right)^{1.4}$$ ————————— HUTH

$$\frac{P}{d} = 2.38 \left(\frac{\rho_p}{\rho_t}\right)^{\frac{1}{3}} \left(\frac{\frac{U}{C_t}}{3 - 1.66\,\frac{U}{C_t}}\right)^{\frac{1}{3}}$$ ——————— VAN VALKENBURG

$$\frac{P}{d} = 2.0 \left(\frac{\rho_p}{\rho_t}\right)^{\frac{2}{3}} \left(\frac{U}{C_t}\right)^{\frac{2}{3}}$$ ——————— A.R.D.E.
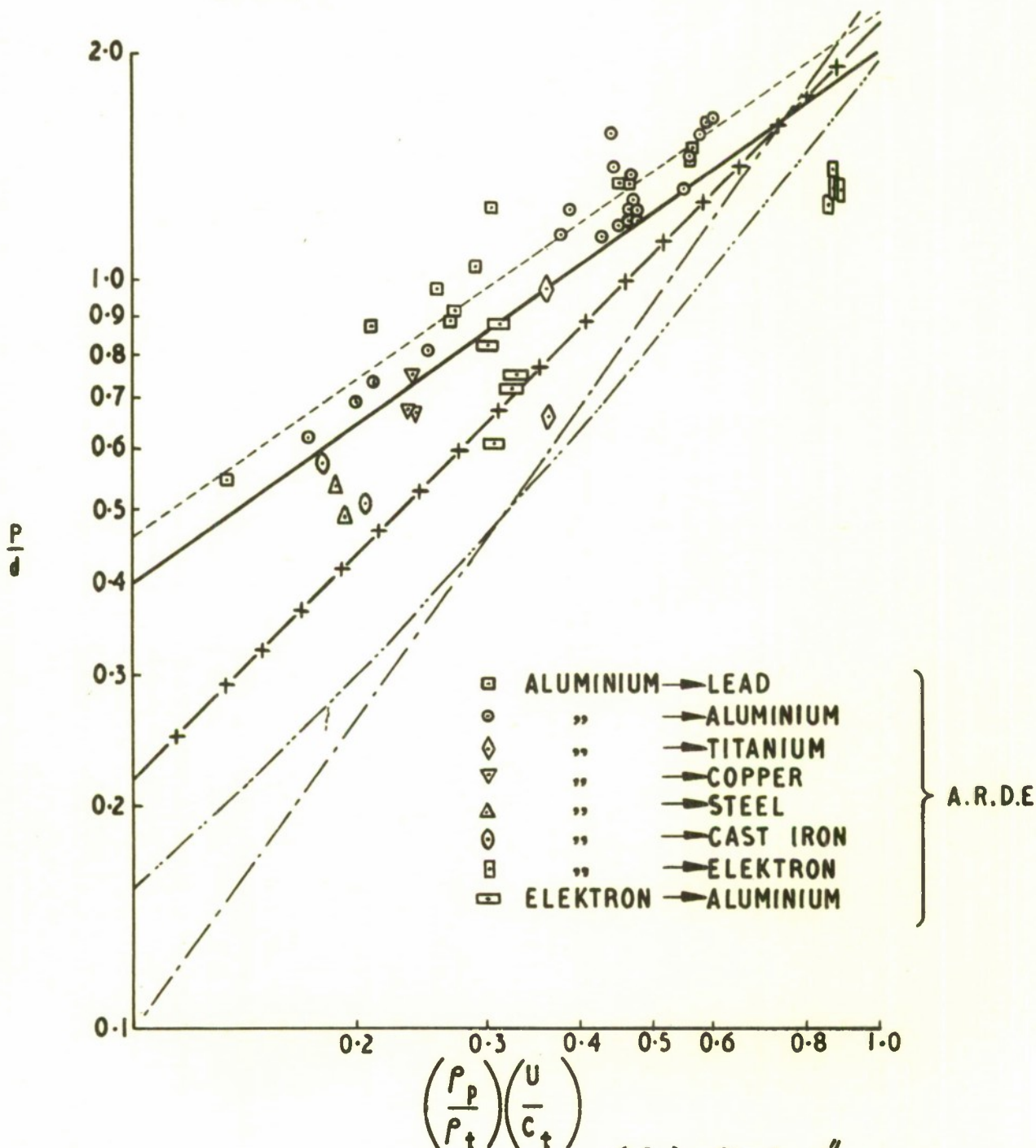
FIG. 3 PENETRATION AS A FUNCTION OF $\left(\frac{\rho_p}{\rho_t}\right)\left(\frac{U}{C_t}\right)$, $\frac{1}{4}''$ SPHERES INTO TARGETS AT NORMAL INCIDENCE

FIG. 4(a)-(e)
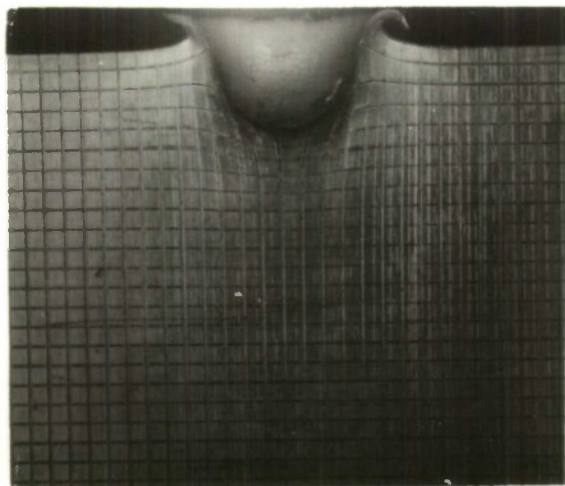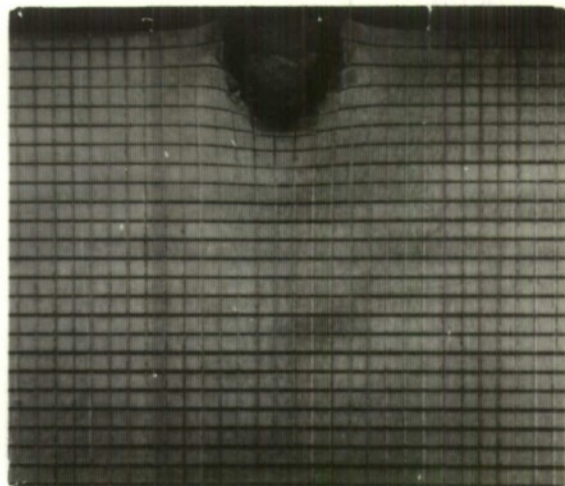
4(a) ALUMINIUM

4(b) ELEKTRON

4(c) CAST IRON
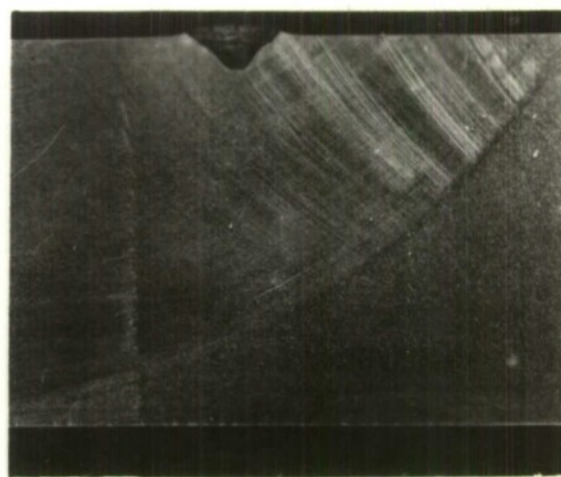
4(d) TITANIUM

END VIEW

SIDE VIEW

4(e) PERSPEX

FIG. 4 TYPICAL CRATERS FORMED IN VARIOUS TARGETS WHEN ATTACKED BY 1/4" DIA. ALUMINIUM SPHERES AT 10,000 FT / SEC
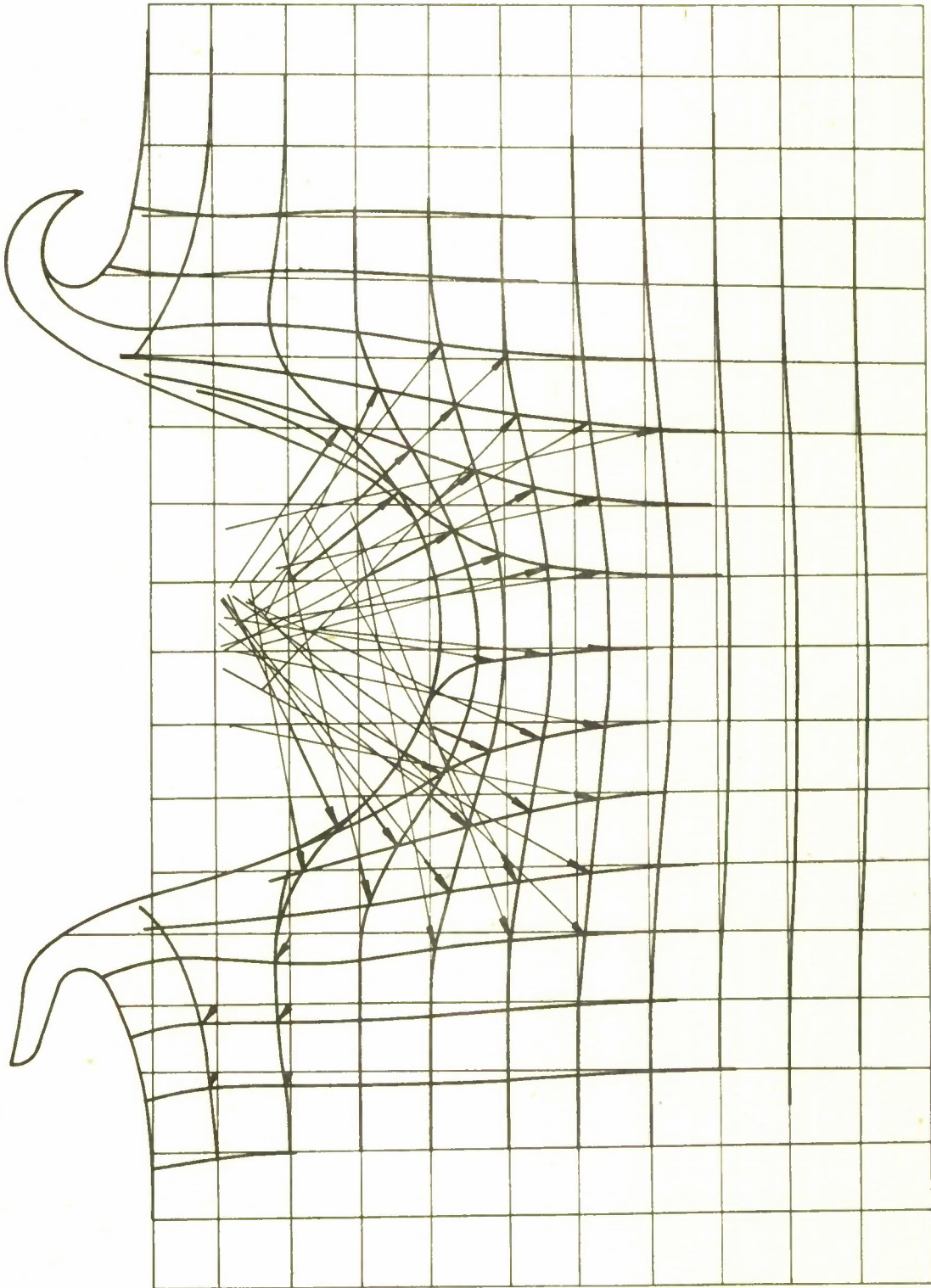
FIG. 5

FIG. 5 PLASTIC DEFORMATION IN AN ALUMINIUM TARGET ATTACKED BY A $\frac{1}{4}$" ALUMINIUM SPHERE AT 10,000 FT/SEC AT NORMAL INCIDENCE

FIG. 5

FIG. 5 PLASTIC DEFORMATION IN AN ALUMINIUM TARGET ATTACKED BY A $\frac{1}{4}''$ ALUMINIUM SPHERE AT 10,000 FT/SEC AT NORMAL INCIDENCE

FIG. 6

$$\left(\delta r\right)^3 + 3r\left(\delta r\right)^2 + 3r^2\left(\delta r\right) - \frac{3\,\delta v}{2\pi} = 0$$

○ δy

⊡ δx
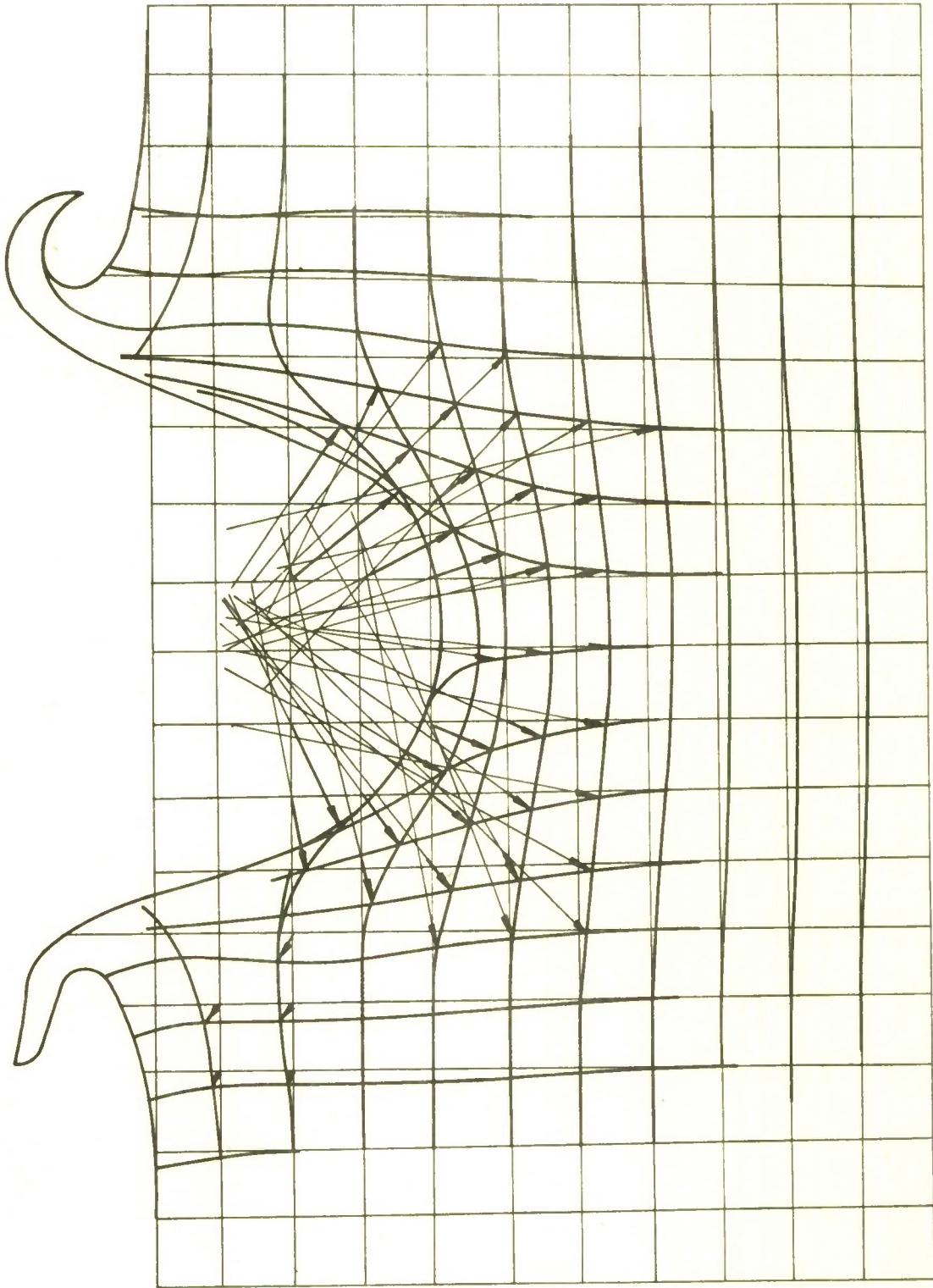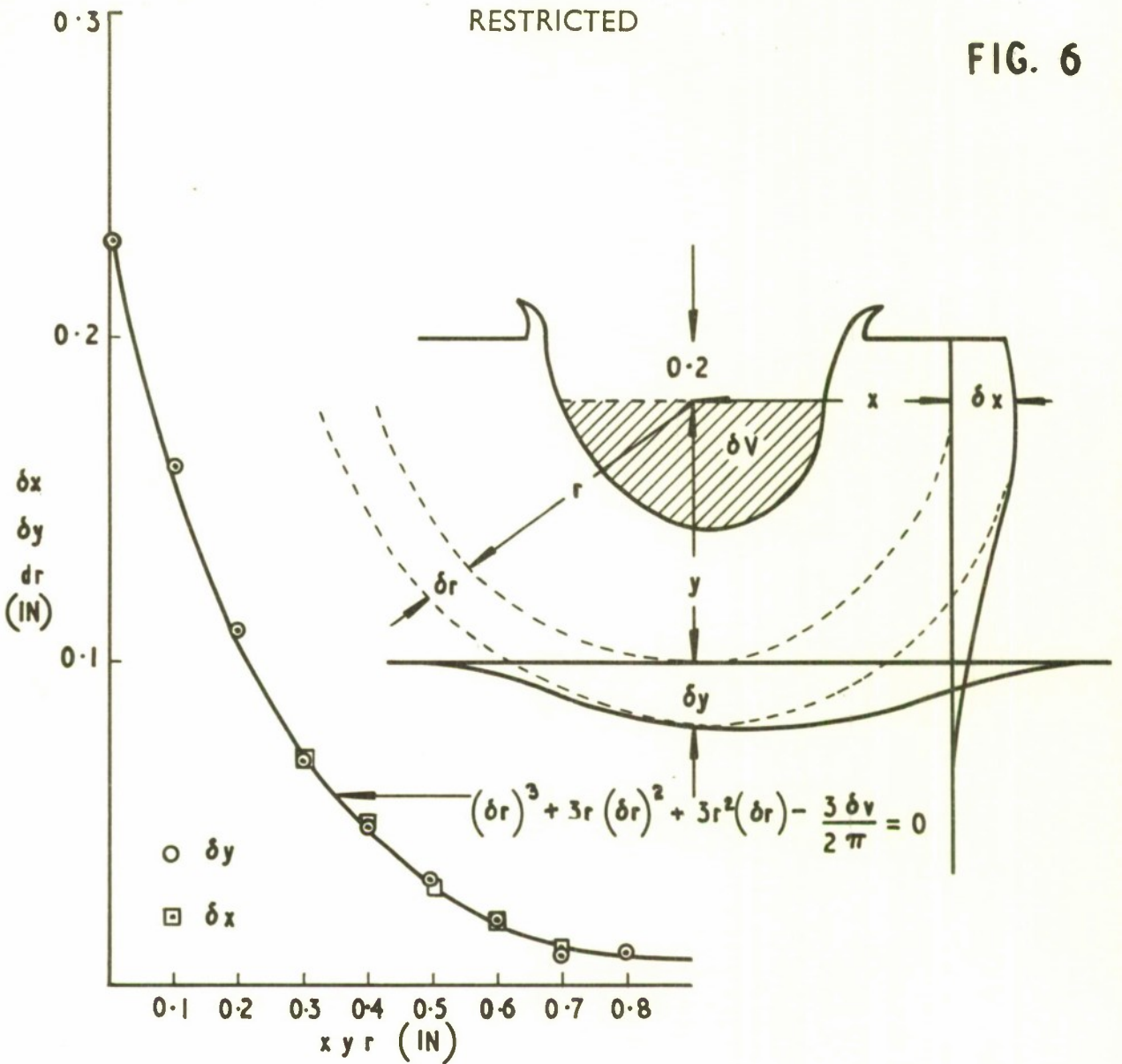
FIG. 6 a   DEFORMATION

$$\epsilon = \frac{d\left(\delta r\right)}{dr}$$
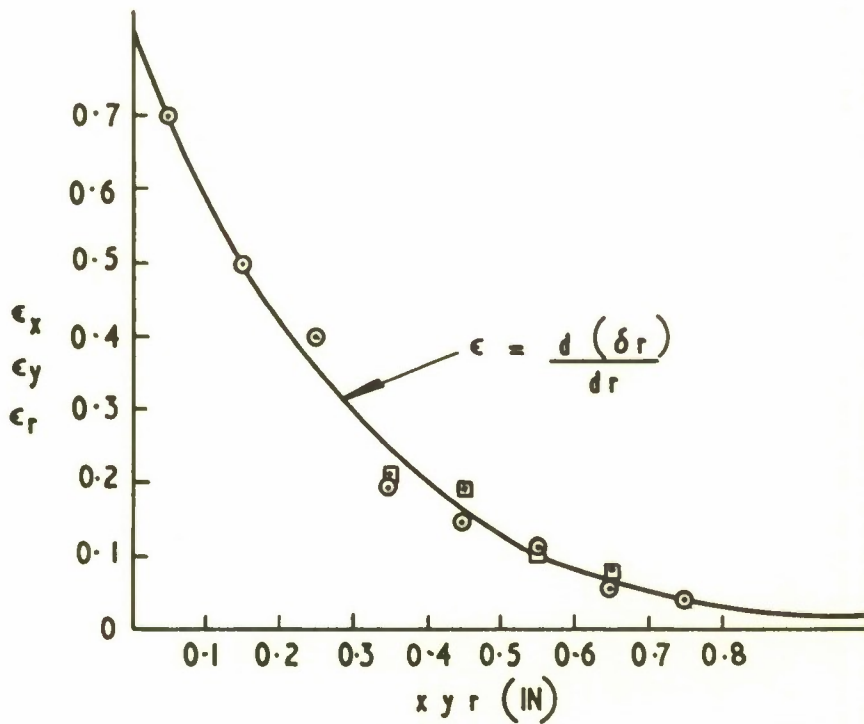
FIG. 6 b   STRAIN

FIG. 6 DEFORMATION AND STRAIN IN AN ALUMINIUM TARGET AT NORMAL INCIDENCE AFTER ATTACK WITH A 1/4" ALUMINIUM SPHERE AT 10,000 FT/SEC.
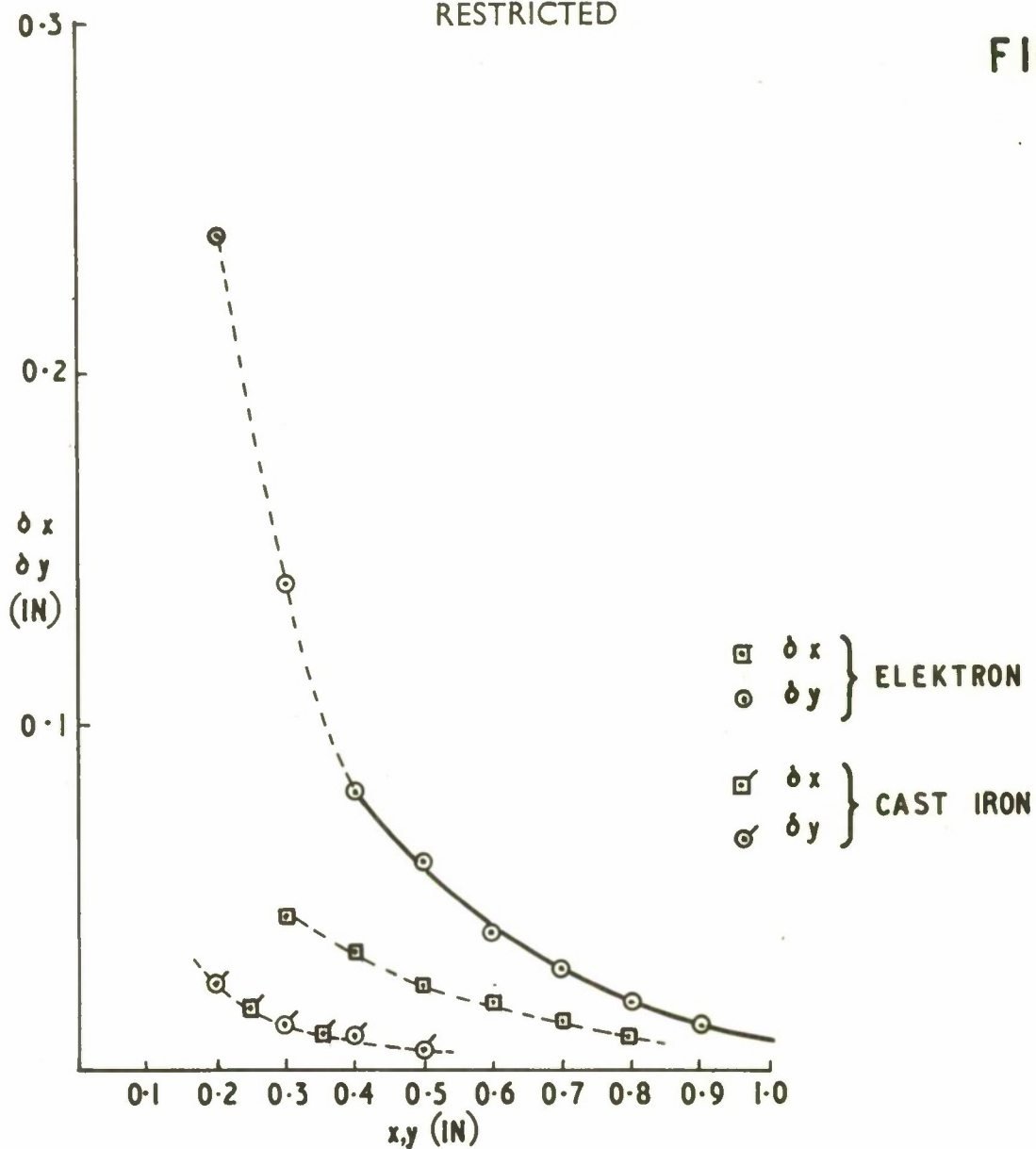
FIG. 7

FIG. 7 a   DEFORMATION
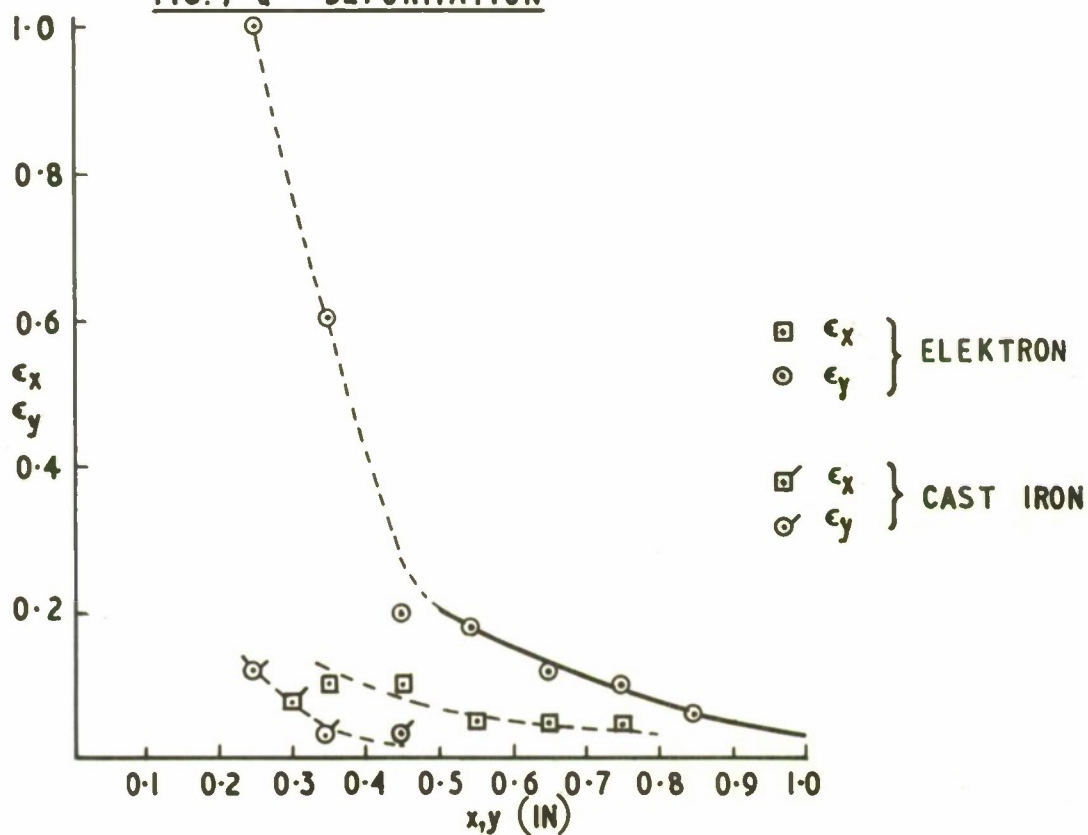
FIG. 7 b   STRAIN

FIG. 7   DEFORMATION AND STRAIN IN ELEKTRON AND CAST IRON
TARGETS AT NORMAL INCIDENCE AFTER ATTACK WITH A
1/4" ALUMINIUM SPHERE AT 10,000 FT/SEC

FIG. 8

$$\frac{P}{d} = \left(\frac{P}{d} \text{ AT } 90° \text{ INCIDENCE}\right) \sin \theta$$

$$\frac{V}{v} = \left(\frac{V}{v} \text{ AT } 90° \text{ INCIDENCE}\right) \sin^2 \theta$$
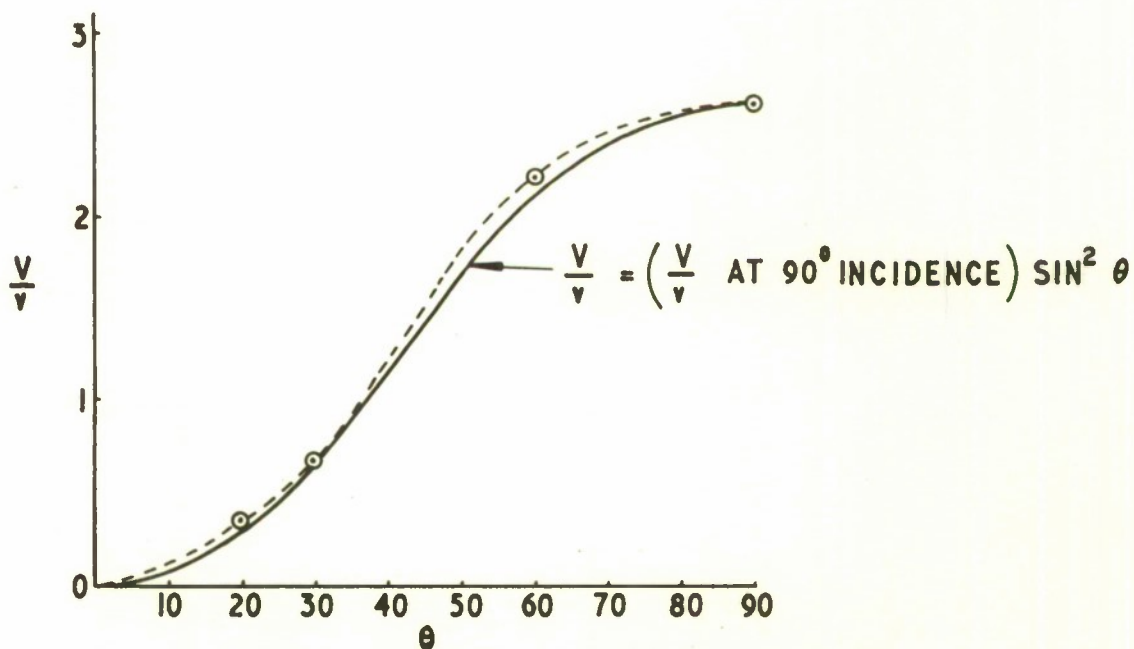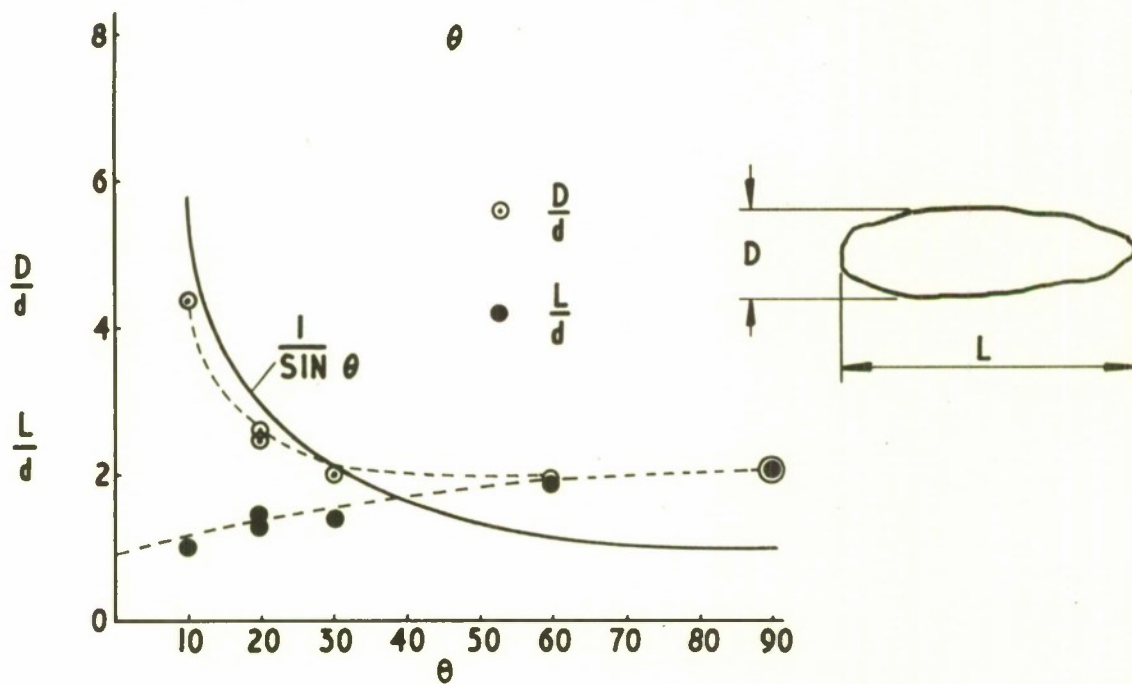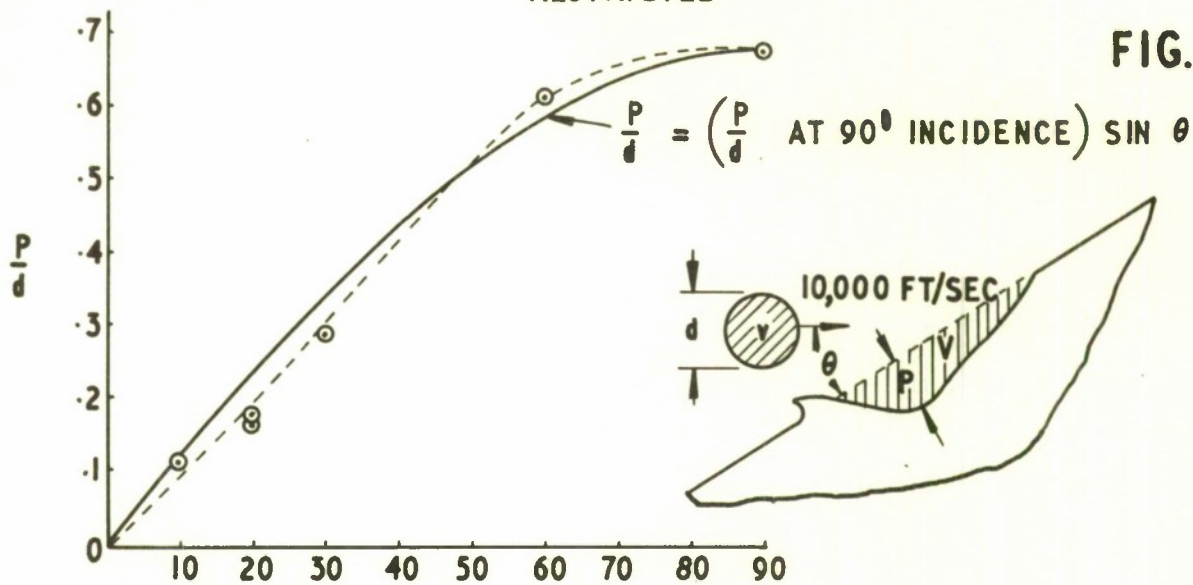
FIG. 8   CRATER   DIMENSIONS   AS   A   FUNCTION   OF   INCIDENCE
$\frac{1}{4}$" ALUMINIUM   SPHERES   INTO   INCLINED   COPPER   TARGETS
AT   10,000   FT/SEC

FIG. 9

$$\frac{P}{d} = \left(\frac{P}{d} \text{ AT } 90° \text{ INCIDENCE}\right) \text{SIN } \theta$$
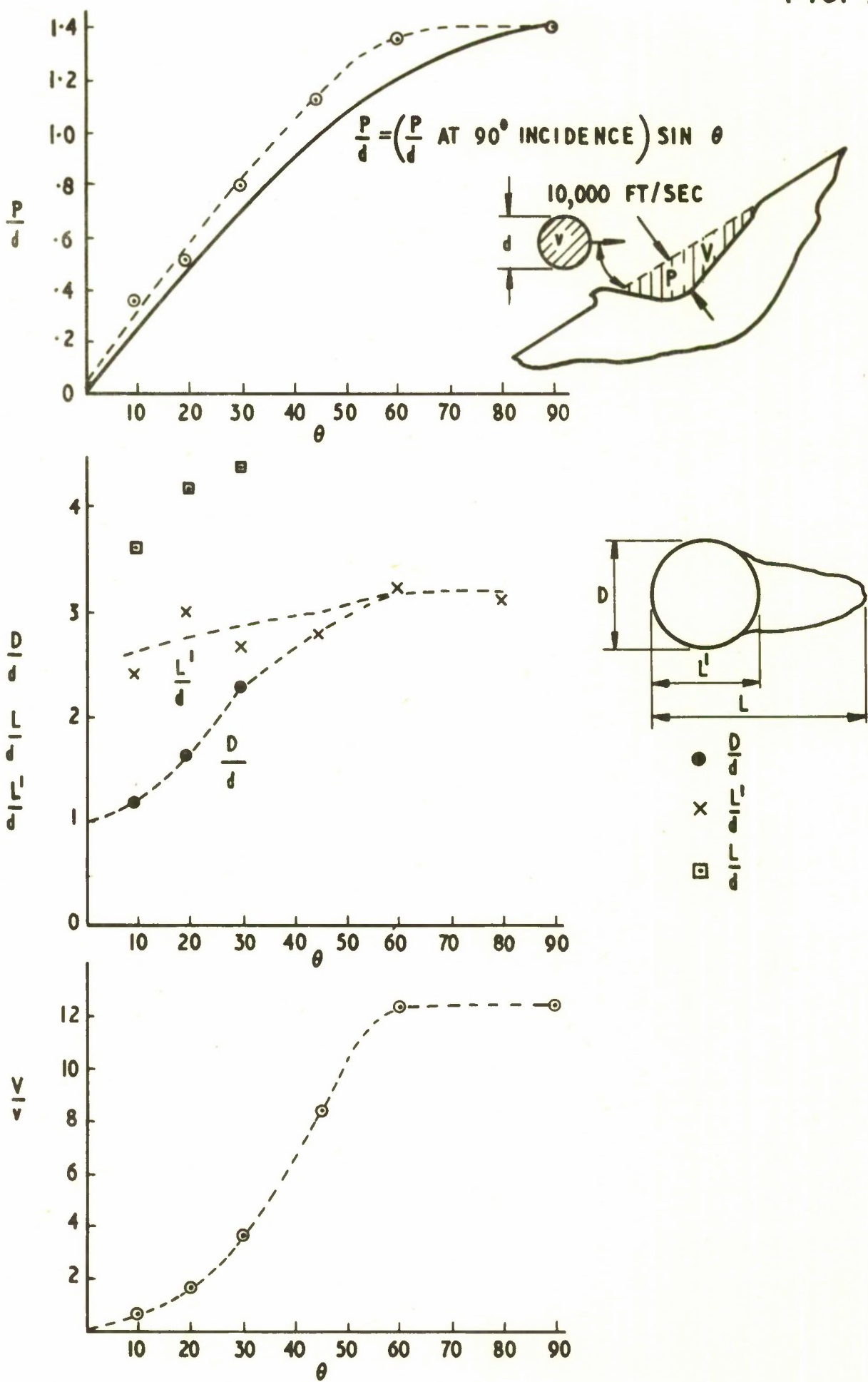
FIG. 9   CRATER   DIMENSIONS   AS   A   FUNCTION   OF   INCIDENCE
1/4″ ALUMINIUM   SPHERES   INTO   INCLINED   LEAD   TARGETS
AT   9,000   FT/SEC.
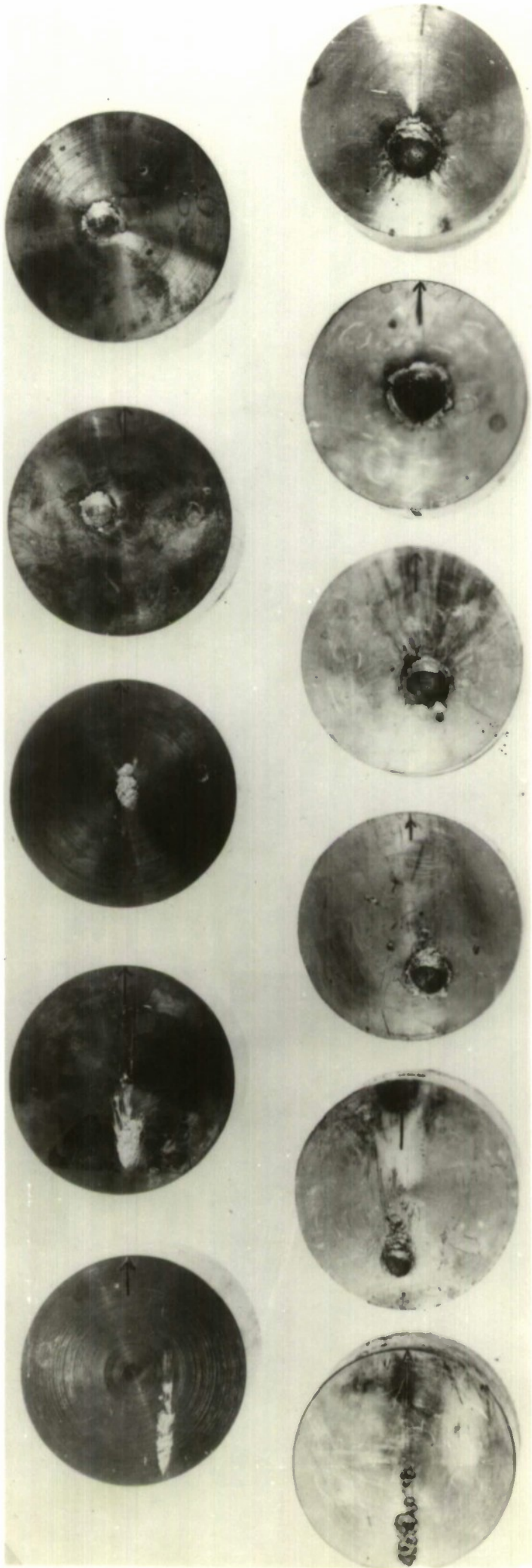
FIG.10

FIG.10 TARGETS AT INCIDENCE

TOP ROW —¼" DIA. ALUMINIUM SPHERES INTO COPPER AT 10,000 FT / SEC.
LEFT TO RIGHT—10°, 20°, 30°, 60°, 90°

BOTTOM ROW —¼" DIA. ALUMINIUM SPHERES INTO LEAD AT 9,000 FT / SEC.
LEFT TO RIGHT—10°, 20°, 30°, 45°, 60°, 90°
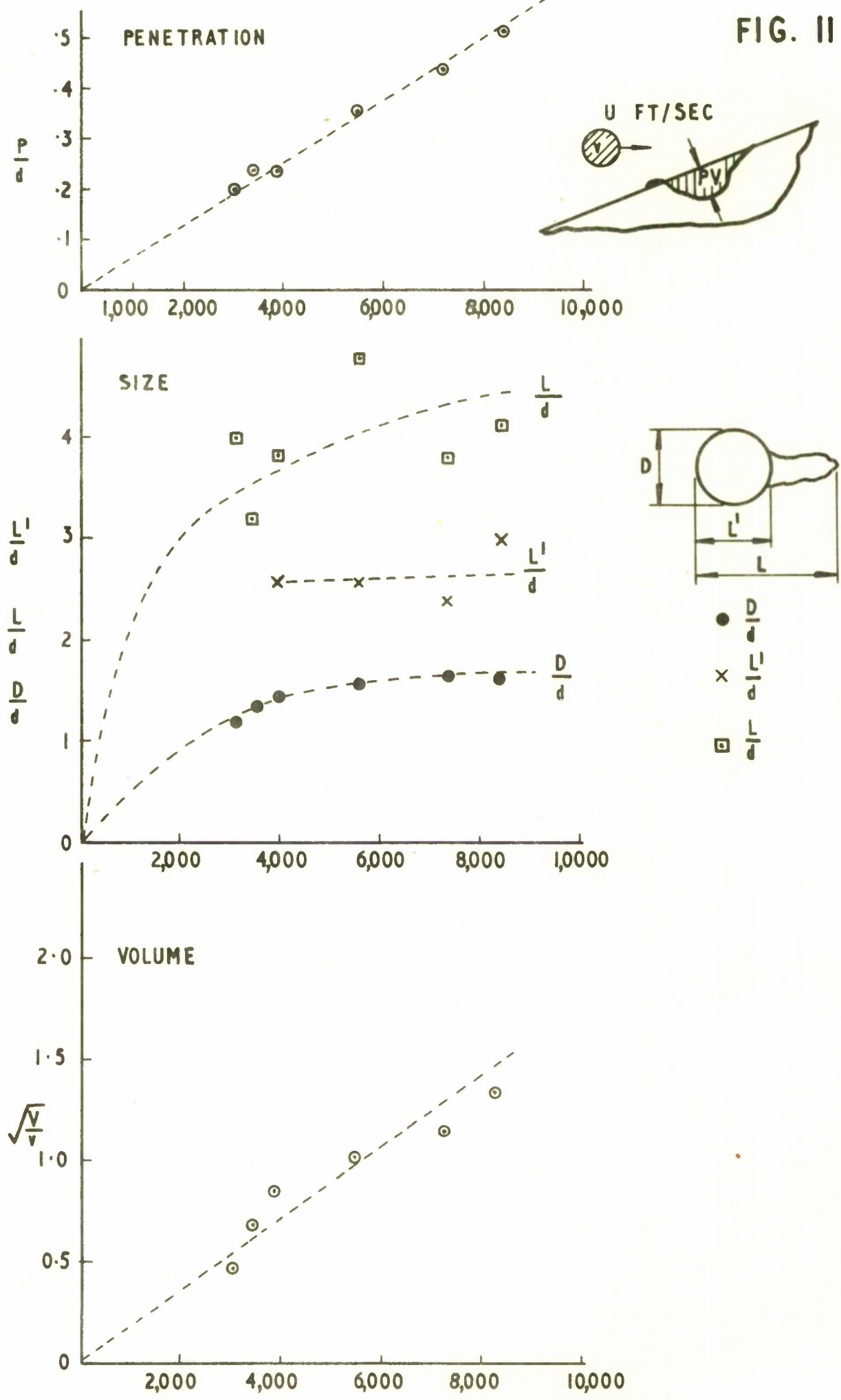
FIG. II CRATER DIMENSIONS AS A FUNCTION OF IMPACT VELOCITY

1/4" ALUMINIUM SPHERES INTO LEAD TARGETS INCLINED AT 20°
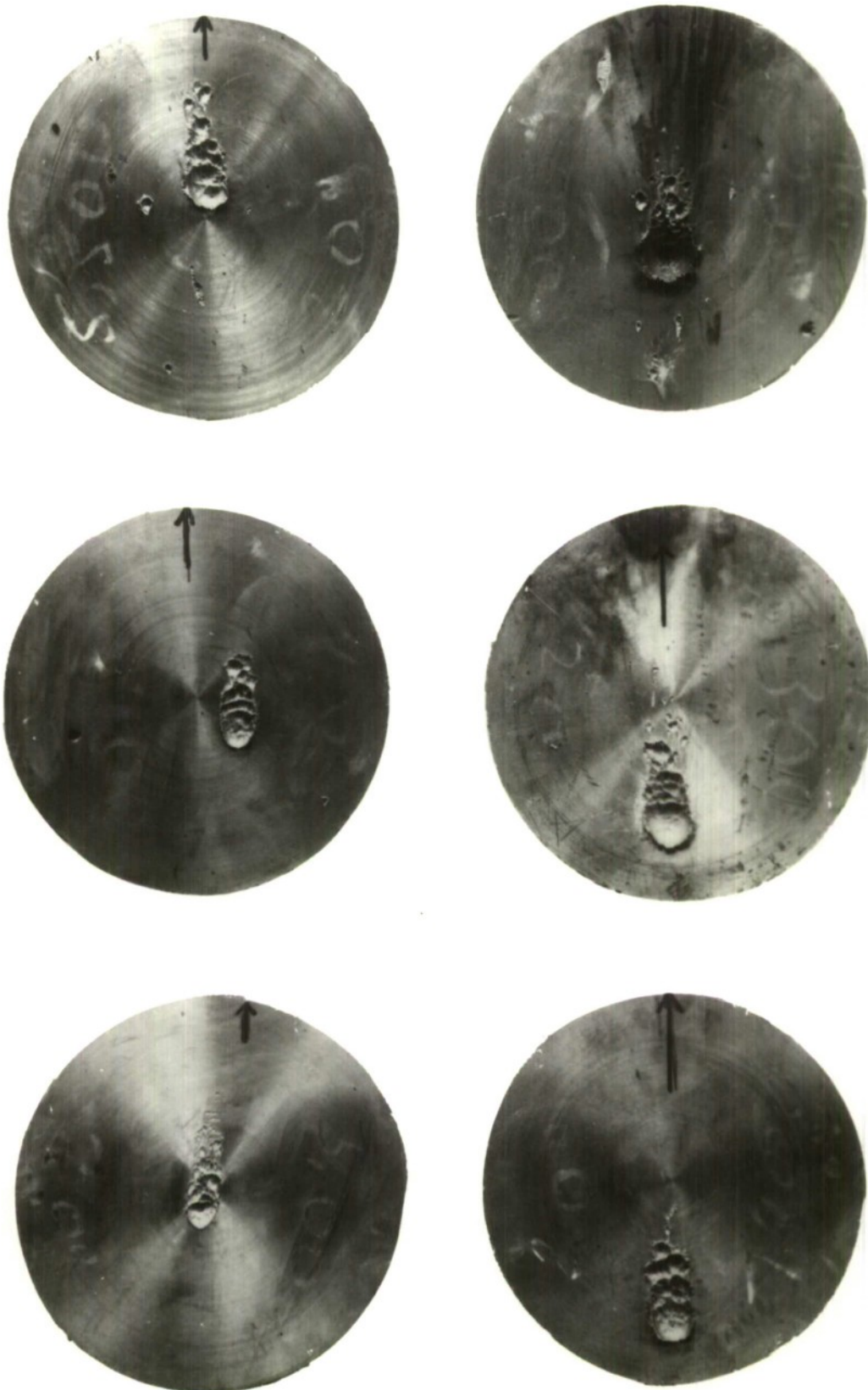
FIG. 12 1/4" DIA. ALUMINIUM SPHERES INTO LEAD TARGETS INCLINED AT 20°
IMPACT VELOCITIES ARE 3,000, 3,900, 5,500, 7,300, 8,300, 11,000 FT/SEC.
INCREASING FROM TOP LEFT TO BOTTOM RIGHT.

FIG. 13
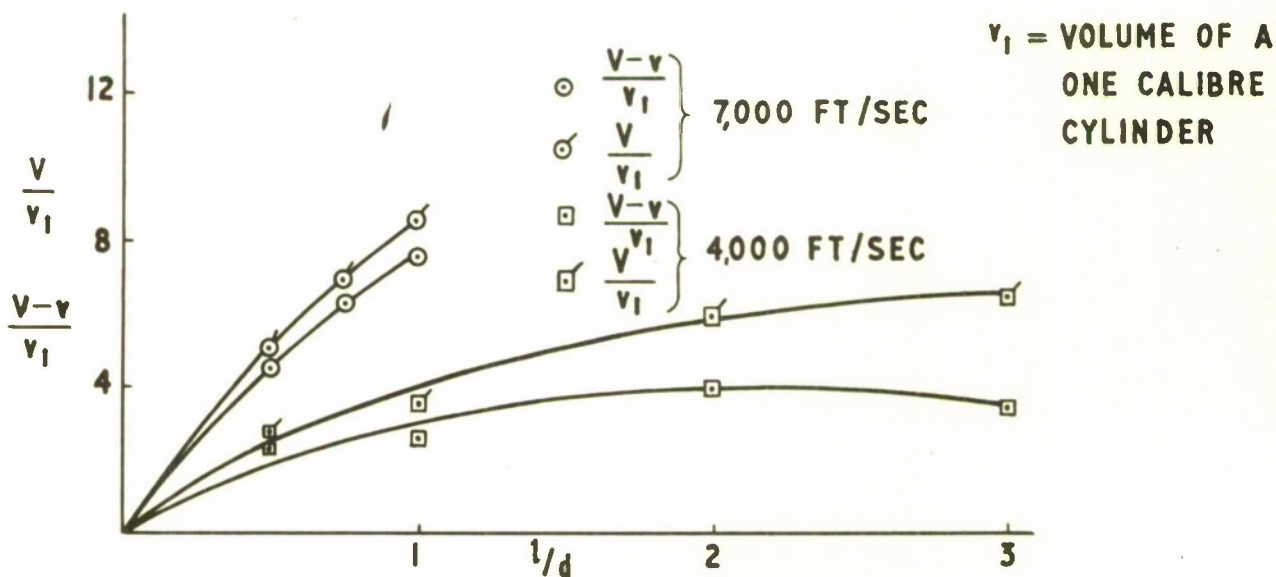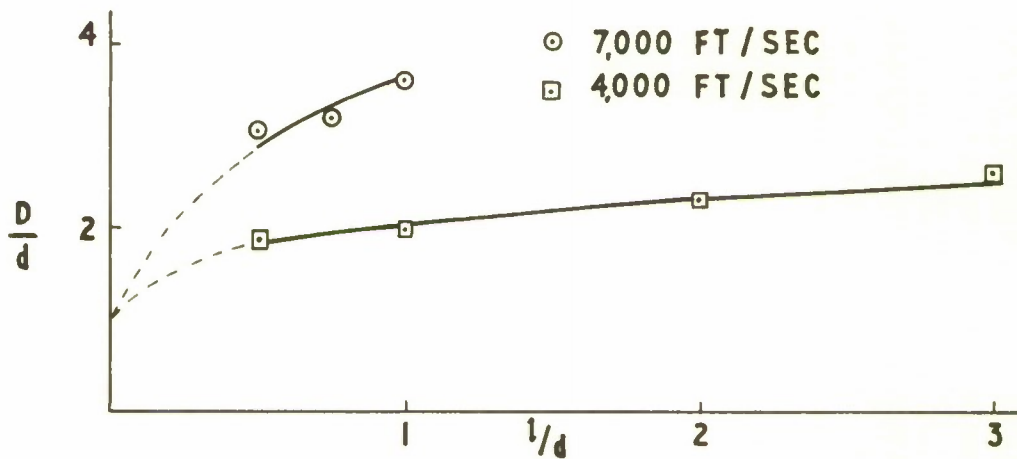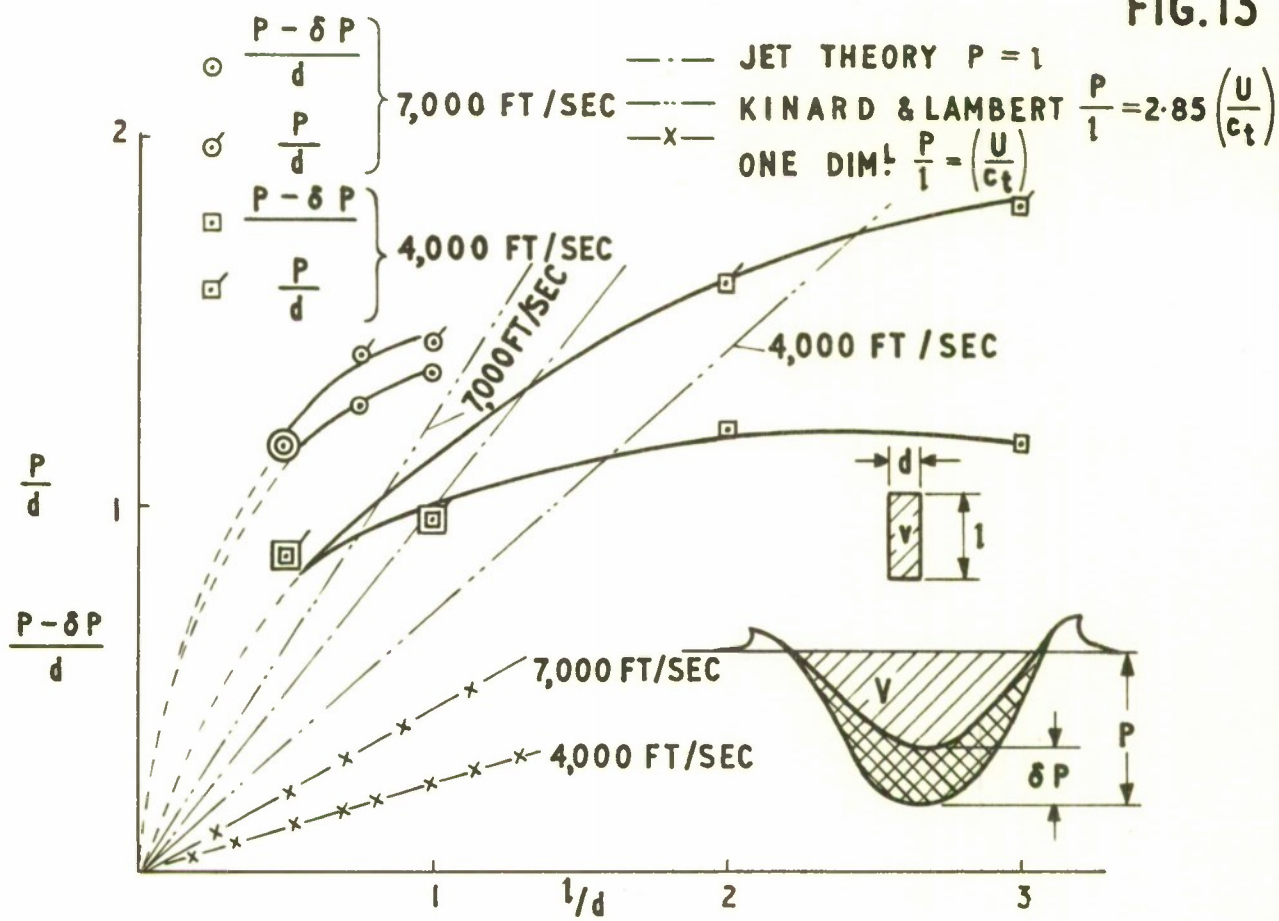
FIG. 13 CRATER DIMENSIONS AS A FUNCTION OF PROJECTILE LENGTH—$\frac{1}{4}''$ ALUMINIUM CYLINDERS INTO ALUMINIUM TARGETS
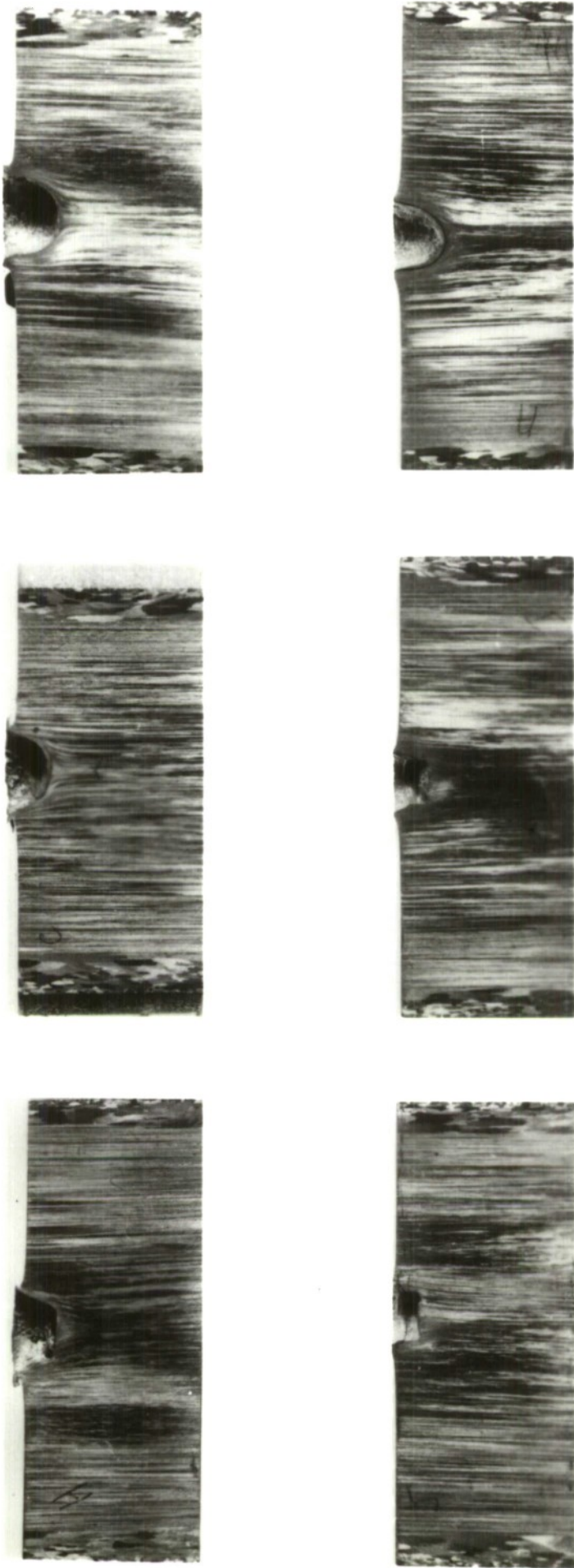
FIG.14

FIG.14 ALUMINIUM CYLINDERS INTO ALUMINIUM TARGETS AT NORMAL INCIDENCE

TOP ROW ——IMPACT VELOCITY 7,000 FT / SEC——FROM L. TO R. 1/2, 3/4 AND 1 CALIBRE PROJECTILES
BOTTOM ROW ——IMPACT VELOCITY 4,000 FT / SEC——FROM L. TO R. 1/2, 1 AND 2 CALIBRE PROJECTILES
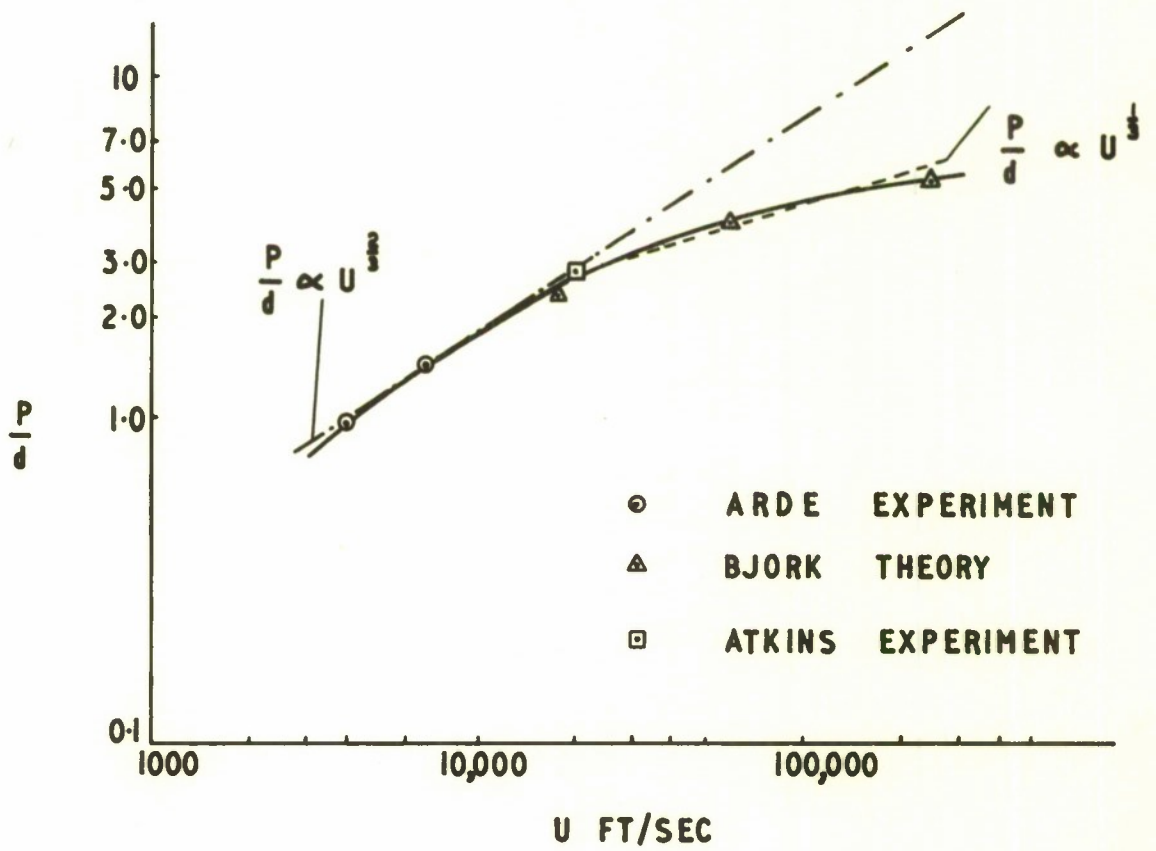
FIG. 15 PENETRATION AS A FUNCTION OF VELOCITY — ONE CALIBRE ALUMINIUM CYLINDERS INTO ALUMINIUM TARGETS
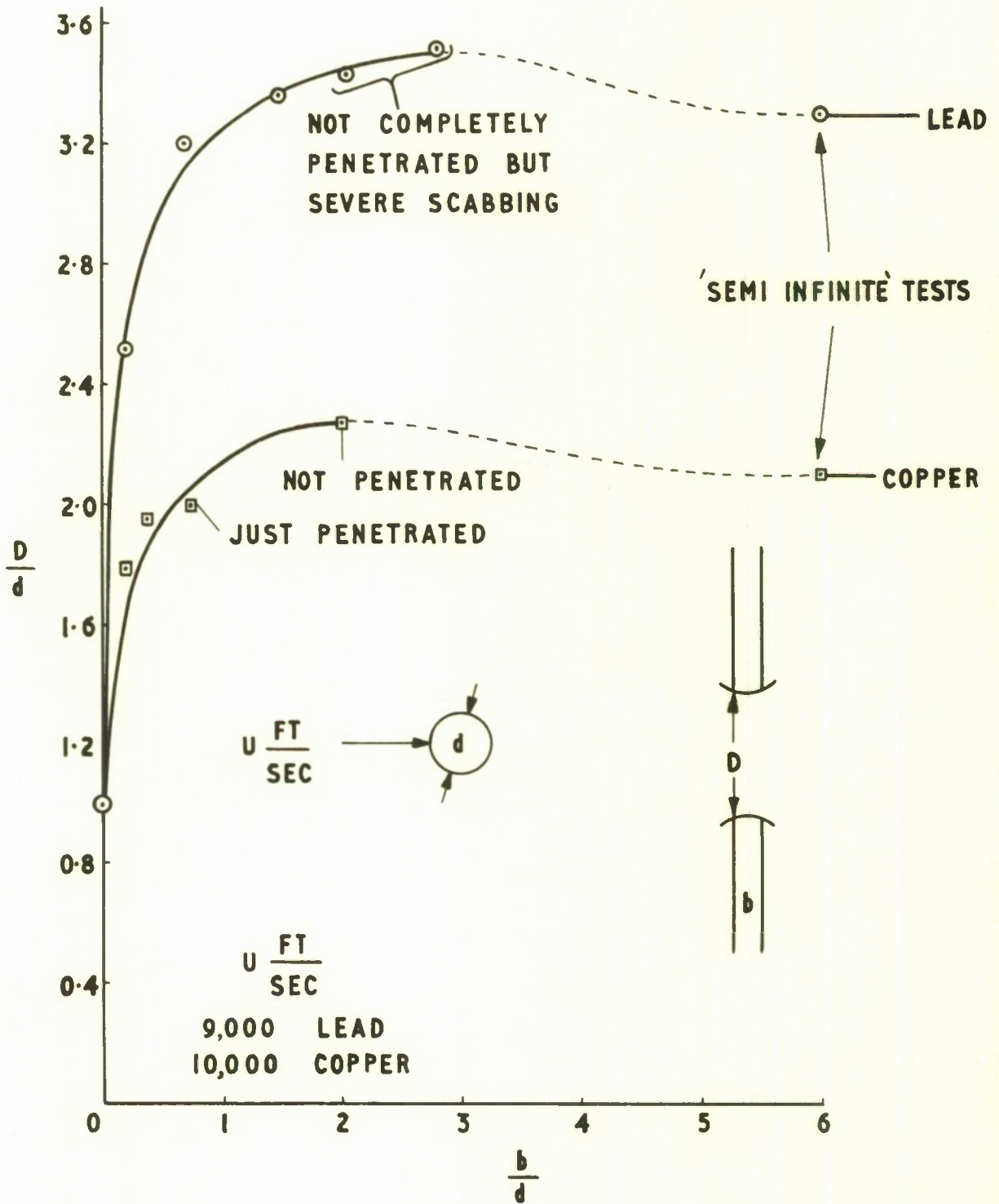
FIG. 16

FIG. 16 CRATER RADIUS AS A FUNCTION OF TARGET THICKNESS, $\frac{1}{4}$" ALUMINIUM SPHERES INTO THIN LEAD AND COPPER TARGETS AT NORMAL INCIDENCE.

FIG. 17(a)-(c)
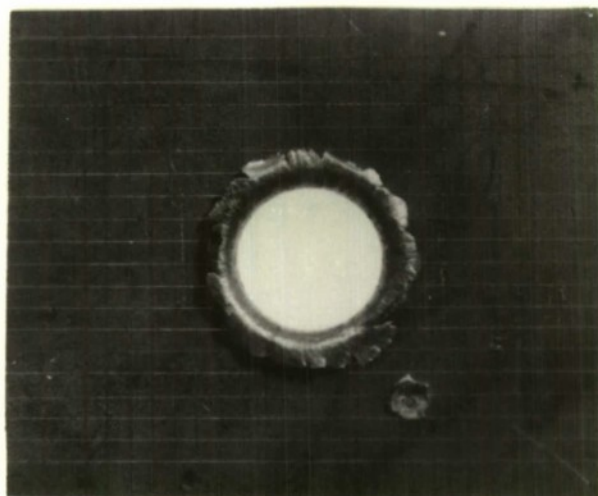
17(a) $\frac{b}{d}$ = 0·2 (FRONT OF TARGET)
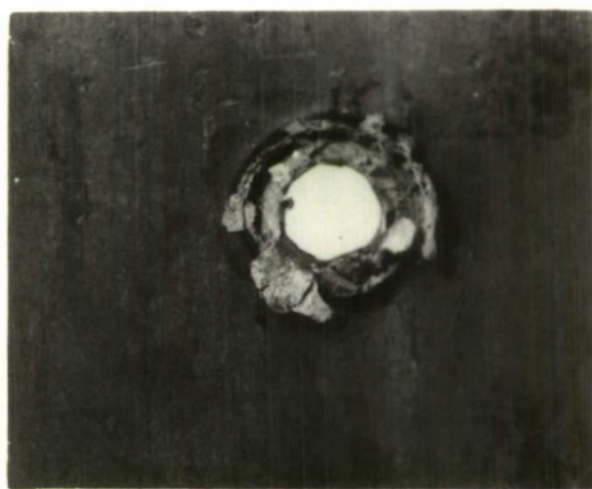
17(b) $\frac{b}{d}$ = 2·05 (BACK OF TARGET)
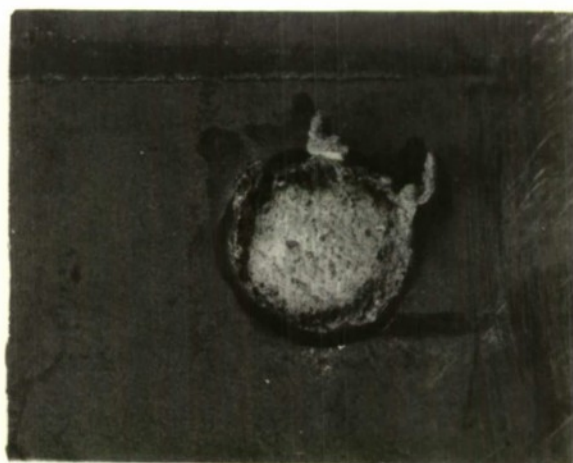
17(c) $\frac{b}{d}$ = 2·8 (BACK OF TARGET)

FIG. 17 CRATERS FORMED IN THIN LEAD TARGETS WHEN ATTACKED AT NORMAL INCIDENCE BY 1/4" DIA. ALUMINIUM SPHERES AT 10,000 FT / SEC.

FIG.18

$$\frac{P}{d} = \left(\frac{P}{d} \text{ AT } 90^\circ \text{ INCIDENCE}\right) \sin \theta$$

$\dfrac{b}{d}$	$\dfrac{L}{d}$	$\dfrac{P}{d}$	$\dfrac{D}{d}$
·187	△		▲
·371	⊡		■
762	⊙		⬮
2·03	◇		◆
6·00	⊙		●

$$\frac{1}{\sin \theta}$$

$$\frac{L}{d}$$

$$\frac{D}{d}$$

CRITERION FOR PENETRATION

○ NOT PENETRATED

× PENETRATED

$$\frac{b^*}{d} = 2 \cdot 75 \left(\frac{U}{c_t}\right)^{\frac{2}{3}} \left(\frac{\rho_p}{\rho_t}\right)^{\frac{2}{3}} \sin \theta$$

$$\frac{b^*}{d} = 3 \cdot 47 \left(\frac{U}{c_t}\right) \left(\frac{\rho_p}{\rho_t}\right) \sin \theta$$

JUST PENETRATED
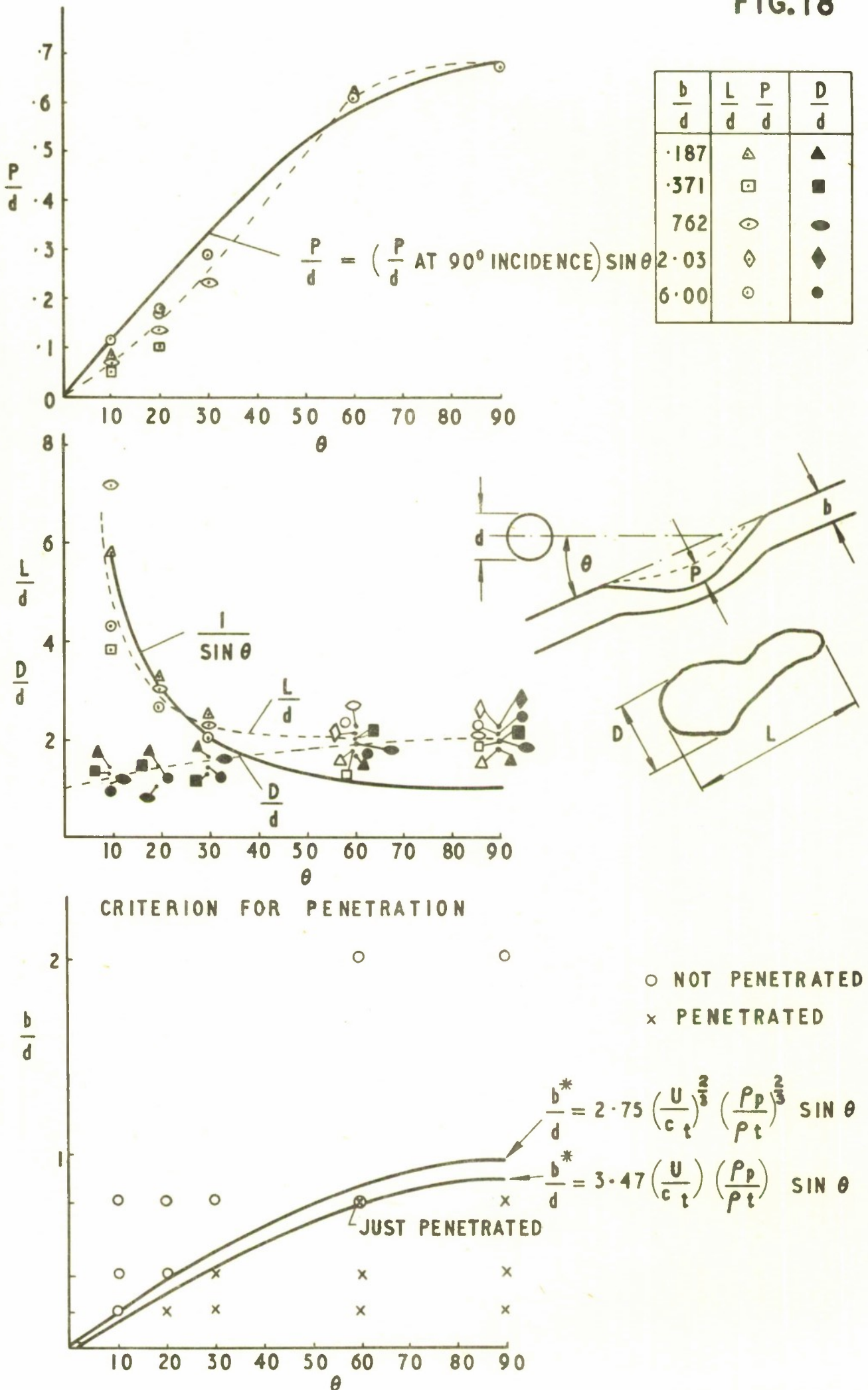
FIG. 18   CRATER DIMENSIONS AS A FUNCTION OF INCIDENCE
¼" ALUMINIUM SPHERES INTO INCLINED THIN COPPER
TARGETS AT 10,000 FT/SEC

FIG. 19

$$\frac{b^*}{d} = 3.47 \left(\frac{U}{c_t}\right)\left(\frac{\rho_p}{\rho_t}\right) \sin \theta$$

$$\frac{b^*}{d} = 2.75 \left(\frac{U}{c_t}\right)^{\frac{2}{3}}\left(\frac{\rho_p}{\rho_t}\right)^{\frac{2}{3}} \sin \theta$$

⊙ NOT PENETRATED

× PENETRATED

CRITERION FOR PENETRATION
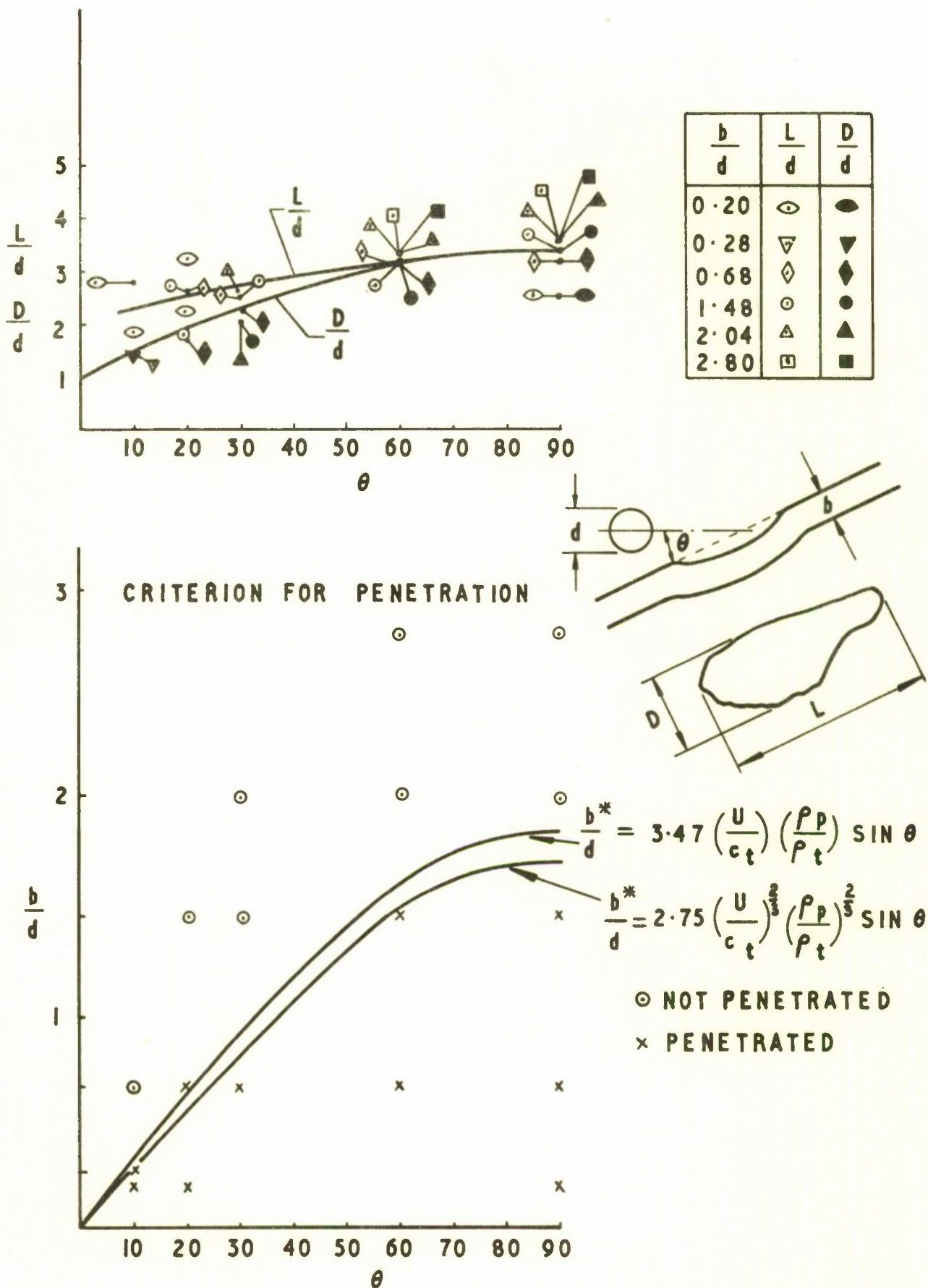
FIG. 19 CRATER DIMENSIONS AS A FUNCTION OF INCIDENCE ¼" ALUMINIUM SPHERES INTO INCLINED THIN LEAD TARGETS AT 9,000 FT/SEC.

RESTRICTED

Defense Technical Information Center (DTIC)
8725 John J. Kingman Road, Suit 0944
Fort Belvoir, VA   22060-6218
U.S.A.

AD#: AD325537

Date of Search: 11 December 2008

Record Summary: DEFE 15/960
        Title: Experiments on hypervelocity impact
        Availability Open Document, Open Description, Normal Closure before FOI Act: 30 years
        Former reference (Department) Memorandum No (B)49/61
        Held by The National Archives, Kew

This document is now available at the National Archives, Kew, Surrey, United Kingdom.

DTIC has checked the National Archives Catalogue website (http://www.nationalarchives.gov.uk) and found the document is available and releasable to the public.

Access to UK public records is governed by statute, namely the Public Records Act, 1958, and the Public Records Act, 1967.
The document has been released under the 30 year rule.
(The vast majority of records selected for permanent preservation are made available to the public when they are 30 years old. This is commonly referred to as the 30 year rule and was established by the Public Records Act of 1967).

This document may be treated as <u>UNLIMITED</u>.